A Study on the Feasibility of Using Fractional Differential Equations for Roll Damping Models

Divyanshu Agarwal

Thesis submitted to the Faculty of the

Virginia Polytechnic Institute and State University

in partial fulfillment of the requirements for the degree of

Master of Science

in

Aerospace Engineering

Leigh McCue, Chair

Cornel Sultan

Craig Woolsey

April 30, 2015

Blacksburg, Virginia

Keywords: Fractional Differential Equation, Damping, Roll, Pitch

A Study on the Feasibility of Using Fractional Differential Equations for Roll Damping Models

Divyanshu Agarwal

(ABSTRACT)

An optimization algorithm has been developed to study the effectiveness of substituting time tested ODEs with FDEs as applied to ship motions, specifically with an eye toward modeling different forms of roll damping. Relations between the order of differentiation a and damping coefficient b in the FDEs have been drawn for changing damping, added moment of inertia, and initial roll angle. A pitch model has also been studied and compared to the roll model. The error at each of these a and b pairs has also been calculated using an L2-norm. An initial effort was made to correlate the FDE coefficients to differing mechanisms of roll damping as characterized by Himeno.

This work was supported by Drs. Patrick Purtell, Ki-Han Kim, and Thomas Fu under the Office of Naval Research (ONR) Grant N00014-10-1-0398 and by Drs. Eduardo Misawa and Massimo Ruzzene under National Science Foundation (NSF) grant CMMI 0747973.

Dedication

To my dearest mom and dad

who love and support me unconditionally

Acknowledgments

I would like to express my appreciation and gratitude to all those who helped contribute to this research and made it a reality. First and foremost I would like to thank my advisor, Dr. Leigh McCue for taking me on as a grad student when I was unsure of what direction to take. She always had an interesting problem available for me to tackle, and whenever I hit a roadblock, she always directed me towards the perfect resources. Thank you Dr. McCue for sticking with me and guiding me till the end.

I would also like to thank Drs. Cornel Sultan and Craig Woolsey for serving on my advisory committee. Dr. Sultan taught a majority of the dynamics and controls courses I took at Virginia Tech and he was the person who truly got me interested in this field. Dr. Woolsey guided me when I suddenly found myself without an advisor and helped me get in touch with Dr. McCue for which I am eternally grateful. I would also like to thank Dr. Troy Henderson for advising me in my first year of grad school and for teaching some of my favorite classes at Virginia Tech.

Finally, I would like to thank my mom and dad, my girlfriend Sarah, my roommate Brian and all my friends, particularly Vidhika and Maggie, for their unwavering love and support. I could not have accomplished this without the constant encouragement you all provided.

Contents

List of Figures

List of Tables

Chapter 1

Introduction

1.1 Motivation

Fractional Differential Equations (FDEs) are an intriguing approach to modeling dynamic systems that have recently received attention in the fields of viscoelasticity, diffusive transportation, rheology, electrical networks, electromagnetic theory, etc. [3]. Despite this, they are not a new concept and were first formally stated in 1695, when L'Hopital questioned the meaning of

$$d^n y/dx^n \tag{1.1}$$

if n is fractional. Unlike integer-order derivatives and integrals which are comparatively easy to visualize, fractional-order calculus does not have a clear physical and geometric interpretation. Despite this, the usefulness of FDEs cannot be overstated since they help capture the memory effects in the system. The convolution integral in the FDE accounts for the presence of past motions and therefore computes the effects from preceding occurrences.

FDEs have been used to analyze vessel motions in the past. Spyrou, Niotis, and Panan-

gopoulou [20] used them to study linear and uncoupled ship rolling. The focus of this paper is to build on the work done in the past and to better understand the implications of replacing time-tested ODEs with the not as common FDEs. This thesis also looks into different cases to help determine situations in which FDEs can substitute ODEs more easily than others. Finally, an attempt is made to obtain a pattern in the fractional values so that these may be calculated in the future without having to run an optimizing routine.

1.2 Problem Definition

A common simplification of the rolling motion in a ship is to compare it to a rotational oscillator as demonstrated by Froude in 1861 [6]. In 1898, Kriloff developed "strip theory" and extended this analogy to encompass all other ship motions as well (subject to limitations) [14]. However these theories were developed based on distinctive terms for inertia, damping, and stiffness [20]. To account for the effects of frequency on hydrodynamic inertia and damping FDEs may be used. FDEs may be able to capture the combined added mass and damping effects, potentially with some amount of system memory, allowing for a more unified approach to these kind of problems.

1.3 Approach

It is not immediately obvious how best to solve an FDE; there are a few different definitions that exist today, however for this thesis, the method developed by Euler in 1730 was chosen. In this approach [3], start with Euler's generalized formula:

$$\frac{d^{\mu}x^{\lambda}}{dx^{\mu}} = \lambda(\lambda-1)...(\lambda-\mu+1)x^{\lambda-\mu} \tag{1.2}$$

Then, with the Gamma function defined as:

$$\Gamma(z) = \int_0^\infty e^{-t} t^{z-1} dt, \qquad Re(z) > 0 \tag{1.3}$$

and using the following property of the Gamma function,

$$\Gamma(\lambda + 1) = \lambda(\lambda - 1)...(\lambda - \mu + 1)\Gamma(\lambda - \mu + 1) \tag{1.4}$$

with some manipulation, one can obtain

$$\frac{d^\mu x^\lambda}{dx^\mu} = \frac{\Gamma(\lambda + 1)}{\Gamma(\lambda - \mu + 1)} x^{\lambda - \mu} \tag{1.5}$$

Many other mathematicians and scientist such as Reimann, Fourier, Liouville, Caputo, etc. also came up with their own definitions for FDEs [3]. The unique approaches have different formulations and limitations. Euler's approach was chosen here since it is a simpler and more fundamental approach and works well for a fractional integer between 0 and 2. This is the area where there is interest in substituting FDEs for ODEs in an effort to capture the frequency dependent hydrodynamic effects in ship motions as identified by Spyrou [20].

1.4 Overview

The remainder of this thesis is laid out as follows. First, a literature review is presented detailing the various methods available for solving FDEs and some of the work done in the past with FDEs. Next, an overview of the roll and pitch equations of motion is presented. The optimization code is explained next before delving into the different components of damping developed by Ikeda and Himeno. Next the trends followed by coefficients a and b

and the related error for a variety of conditions is presented. Finally the FDEs are applied to the pitch model and the results are compared with the roll model.

Chapter 2

Literature Review

In this past decade FDEs have attracted a vast amount of attention. Dalir and Bashour [3] detailed the origins of FDEs and studied the formulation of Euler's approach to FDEs. They also described approaches by Fourier, Abel, Riemann, Sonin *et al.*, Riemann and Liouville, Grünwald and Letnikove, Caputo, and Miller and Boss. Liouville's three different approaches (exponential, fractional integral, and fractional derivative) are also presented by Dalir and Bashour [3]. The presentations of these different approaches and their limitations helped drive the decision of which approach to use in this thesis.

One of the earliest applications of FDEs was conceived by Oliver Heaviside in 1892 in his work on electrical transmission lines [10]. Abel's classic problem in 1920 dealing with tautochronous motion made use of FDEs with a fractional integral to the order of $\frac{1}{2}$ [5]. More recently, Sebaa *et al.* [19] used fractional calculus to detail the interactions between fluid and solid structures. Assaleh *et al.* [1] used fractional calculus to improve an earlier integer order model for speech signals. These works demonstrated the potential for FDEs to replace ODEs effectively and with good accuracy. A similar goal of replacing ODEs with FDEs and predicting future forms of the FDE will be attempted in this thesis.

FDEs have also been used to study dynamic systems and subsequent controls in the past. Suárez *et al.* [21] used FDEs to study the lateral and longitudinal control schemes for autonomous vehicles. Oustaloup [17] used FDEs to develop the CRONE-controller and demonstrated the advantages of this controller over the classical PID-controller. The most relevant example is Spyrou *et al.*'s work [20] in which FDEs were also used to model ship rolling and which inspired the further study conducted in this research.

Further research in the field of ship rolling was conducted by Bassler and Reed [2] who studied and further developed the bilge keel roll damping component. They also applied this damping component to the cargo ship hull form given by Ikeda, *et al.* [12] and Himeno [11]. Dalzell [4] developed an approximation to the conventional mixed linear-plus-quadratic ship roll damping model. With all this theory and earlier applications available, this thesis will attempt to develop a method for approximating the fractional coefficients in FDEs.

Chapter 3

Model

3.1 Roll

While rigid body ship motions would be more fully modeled with a coupled, six degree of freedom set of equations, for purposes of this work, and to glean a fuller understanding of the implications of using fractional differential equations, the focus has been shifted to single degree of freedom motions. A simplified roll equation of motion can be given as in Equation 3.1 [11]:

$$A\ddot{\phi} + B\dot{\phi} + C\phi = 0 \tag{3.1}$$

where A is the actual moment of inertia plus the added hydrodynamic moment of inertia in roll, B represents the roll damping moment coefficient, and C is the coefficient of hydrostatic restoring moment, taken here to be equal to $mg * GM$. In C, the m is the mass, g is gravity, and GM is the metacentric height.

Thus the above equation can be rewritten as the ODE:

$$(I + \delta I)\ddot{\phi} + b\dot{\phi} + mgGM\phi = 0 \tag{3.2}$$

where I is the mass moment of inertia and b is the damping. The δI is the added mass moment of inertia and has been included in the ODE as done in the past by many [24] [15] [23]. It should also be noted that the ODE considered is unforced.

For comparison, an FDE as presented in Equation 3.3 is sought to model the ODE approach, where the order of the fractional derivative is expected to capture added inertia and damping effects. This approach is consistent with Spyrou [20].

$$I\ddot{\phi} + bD^{(a)}\phi + mgGM\phi = 0 \tag{3.3}$$

Equation 3.3 (FDE) above can be used to reasonably reproduce Equation 3.2 (ODE) through optimally selecting values of a and b.

The model used in this thesis is from a series of towing tank experiments by Takaki and Tasai in 1973 [22]. The dimensions of the model are detailed in Table 3.1.

Viewing this model as a box barge allows it to be simplified to a rectangular cross section. This makes calculations of the mass moment of inertia and the added moment of inertia straight forward. The mass moment of inertia can be calculated using Equation 3.4:

$$I = \frac{1}{12}m(B^2 + d^2) \tag{3.4}$$

where m is the mass of the ship, B is the breadth, and d is the draft. This results in a mass moment of inertia of 4.4476 kg m^2 for the rolling model of the ship.

Table 3.1: Dimensions of the model per Takaki and Tasai
Takaki, M., & Tasai, F. (1973). On the Hydrodynamic Derivative Coefficients of the Equations for Lateral Motions of Ships, *T West-Japan SNA*, Vol. 46. Used under fair use, 2015.

	Cargo Ship
Length, L_{PP} (m)	3.00
Breadth, B(m)	0.4783
Draft, d(m)	0.1957
Displacement, Δ(kg)	199.84
C_B	0.7119
C_M	0.9905
GM (m)	0.02174
OG (m)	-0.025
K_L/L_{PP}	0.2172
KB/B	0.3240
l_{BK}/L_{PP}	0.25
b_{BK}/B	0.0159

3.2 Pitch

For the pitching model of the ship some of the values need modifications. For the new mass moment of inertia, the breadth, B in Equation 3.4 must be replaced with the length, L_{PP} resulting in a mass moment of inertia of 150.5178 kg m^2. The GM values in Equation 3.2 and Equation 3.3 must also be adjusted accordingly for pitching. In this case, the longitudinal metacentric height GM_L must be used instead which is calculated using Equation 3.5 by Gillmer and Johnson [8]:

$$GM_L = KB + BM_L - KG \tag{3.5}$$

where KB is the vertical distance from the keel to the center of buoyancy, BM_L is the longitudinal metacentric radius, and KG is the vertical distance from the keel to the center of gravity. BM_L is calculated using Equation 3.6 by Gillmer and Johnson [8]:

$$BM_L = \frac{I_L}{\nabla} \tag{3.6}$$

where I_L is the longitudinal moment of inertia and ∇ is the volume displacement calculated using Equations 3.7 and 3.8 by Zubaly [27]

$$I_L = \frac{L^3 b}{12} \tag{3.7}$$

$$\nabla = LBT \tag{3.8}$$

where L is the length, B the breadth, and T the draft of the ship. This results in a GM_L value of 3.735 m which is over 170 times the transverse GM value. However this is as expected and it is the reason why it is nearly impossible to render a ship unstable longitudinally, particularly a box barge [27].

Chapter 4

Optimization Code

An optimization routine for finding the best-fit a and b values by comparing the FDE model (Equation 3.3) to the ODE model (Equation 3.2) was written in-house and was developed using Matlab version R2013b. The built-in function **ode45** was utilized. The **ode45** command implements the Runge-Kutta method with a variable time step which allows for efficient computation. The Runge-Kutta method numerically integrates ODEs by using a temporary step in the middle of each interval therefore canceling out the lower-order error terms [16]. The **ode45** function is ideal when the problem is in the format of Equation 4.1 as could be obtained here.

$$\frac{dx}{dt} = f(t, x), \quad x(t_0) = x_0 \tag{4.1}$$

where t represents the independent variable, x the vector of dependent variables, $f(t, x)$ denotes a function of t and x, and $x = x_0$ at time t_0 is defined.

Calculating coefficients a and b required starting with the ODE (Equation 3.2). Using the **ode45** function on the ODE returns a time history for the roll angle ϕ (radians) and roll

velocity $\dot{\phi}$ (radians/sec). Next, the **ode45** function was used on the FDE while doing a sweep over the different values of a and b. This results in a large set of time-history vectors for the FDE, one for each combination of a and b. The error for each pair is calculated using Equation 4.2.

$$Error = \sum_{k=1}^{n} abs(x_{ODE_k} - x_{FDE_k}) \tag{4.2}$$

where x is the roll angle (in radians) or roll velocity (in radians/sec) at time step k for the ODE or FDE depending on the subscript, and n is the number of time steps over which the time history was obtained. This approach is often referred to as the L2-norm error. The lowest error yields the optimal combination for the coefficients a and b.

To ensure that the program operates as desired, a simple check is to modify the FDE to also include the added inertia effects. This results in a temporary FDE as follows:

$$(I + \delta I)\ddot{\phi} + bD^{(a)}\phi + mgGM\phi = 0 \tag{4.3}$$

When Equation 4.3 is compared to Equation 3.2 it is apparent that when $a = 1$ and $b_{ODE} = b_{FDE}$ the two equations will be the same, resulting in an error of 0. Since the error cannot be negative, this would be the lowest error and would yield the optimal pair of a and b. Many scenarios were run with a range of different damping values in the ODE and all resulted in the program choosing the right combination of a and b coefficients. Shown here are two examples, one at a lower damping value, and the other at a higher damping value.

The first case presented in Figures 4.1 and 4.2 is where the damping in the ODE is set to 0.4 N m s. The second scenario shown in Figures 4.3 and 4.4 has the ODE damping set to the much higher 4.3 N m s. The added mass moment of inertia for all the roll cases is 0.0973 kg

m^2. As can be seen from the two scenarios, the program correctly chooses $a = 1$ and $b_{ODE} = b_{FDE}$. The error obtained in both these scenarios was 0 as expected. Therefore it can be reasonably concluded that the program is operating as desired.

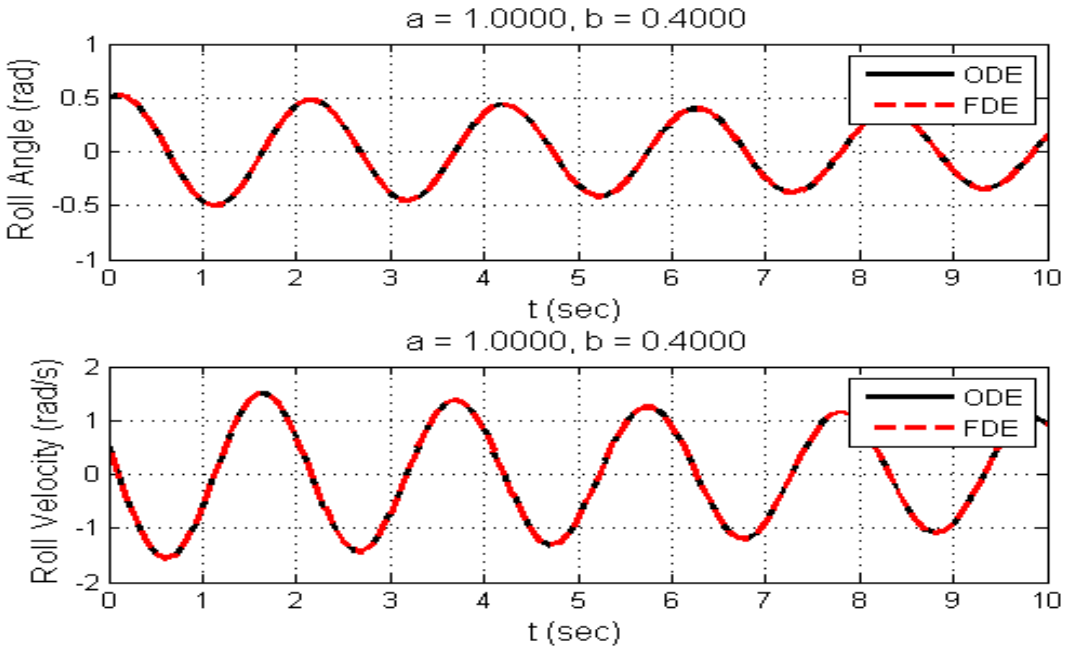

Figure 4.1: Roll angle and roll velocity vs. time when ODE damping = 0.4 N m s

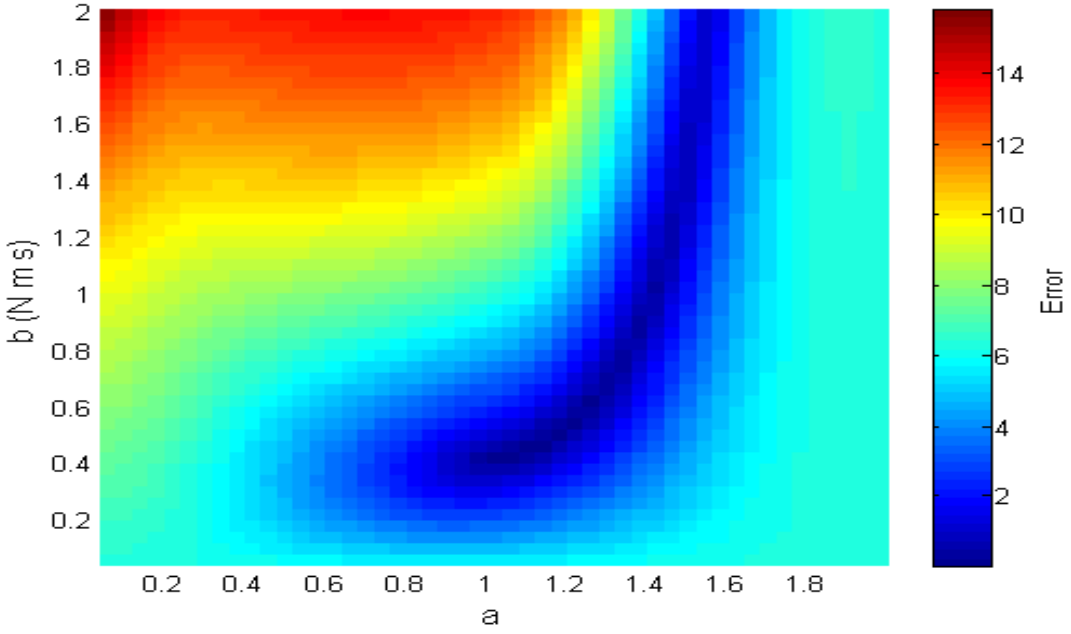

Figure 4.2: Error in roll angle and roll velocity at different numeric values of a and b when ODE damping = 0.4 N m s

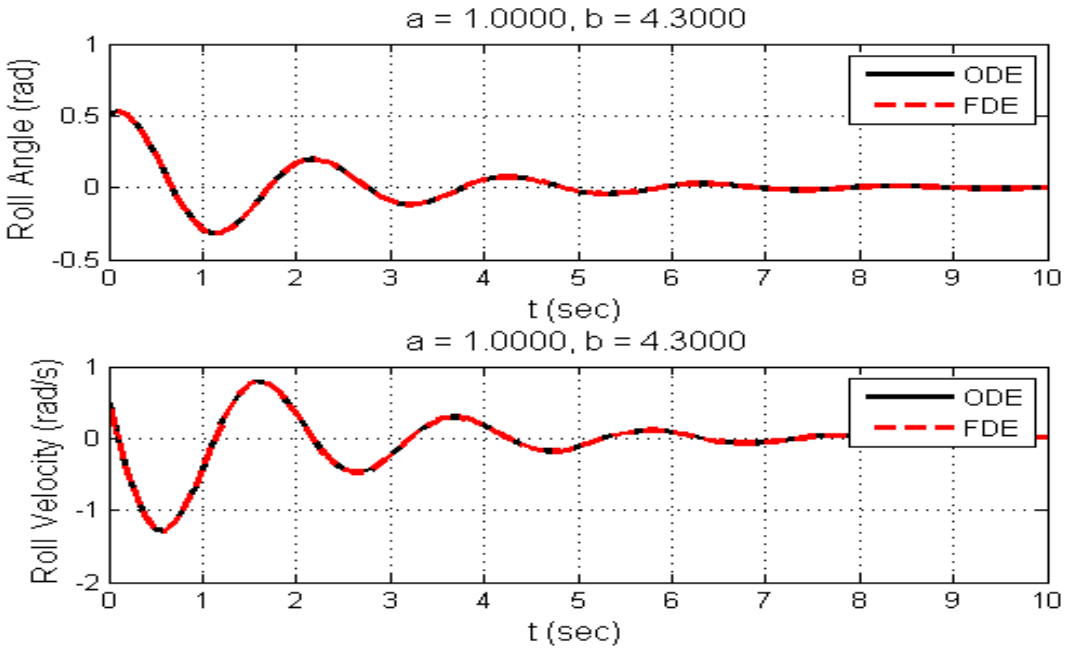

Figure 4.3: Roll angle and roll velocity vs. time when ODE damping = 4.3 N m s

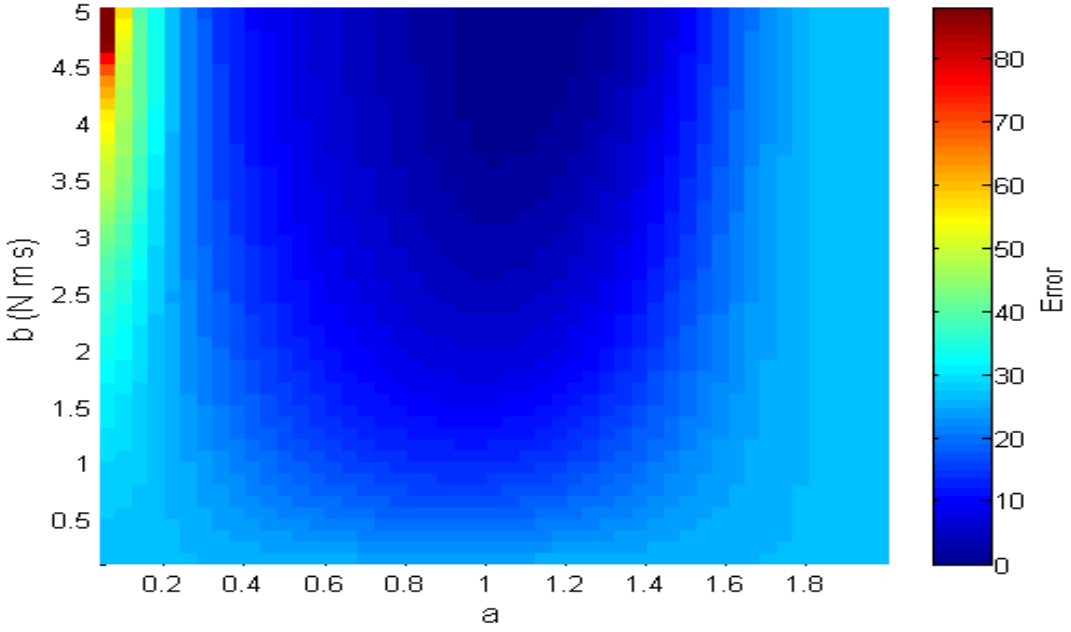

Figure 4.4: Error in roll angle and roll velocity at different numeric values of a and b when ODE damping = 4.3 N m s

Chapter 5

Different Components of Damping

To apply the program verified in the previous chapter to a realistic damping model, Himeno's [11] work on equivalent linear damping was chosen. The equivalent linear damping B_e can be expressed as a sum of five different damping components at a Froude number of 0.2. These five different components are the frictional damping B_F, lift damping B_L, wave damping B_W, and the two different components of the bilge keel damping B_{BK}: the normal force damping of bilge keels B_{BKN}, and the hull pressure damping due to bilge keels B_{BKH}. From Himeno's [11] work, this can be expressed as:

$$B_e = B_F + B_L + B_W + B_{BKN} + B_{HKH} \tag{5.1}$$

Figure 4.16 in Himeno's work [11] demonstrates this damping coefficient for different Froude numbers. For the purpose of this thesis, only a Froude number of 0.2 is considered.

There are two other components of damping too, however they will not be addressed in this study. One of these two components is the eddy damping B_E which is small at a Froude number of 0.2. The other is the third component of bilge keel damping, called the wave

damping of bilge keels B_{BKW}. This is disregarded because it is a very small component of the total damping, it is hard to formulate, and there was no practical data that could be used to validate a calculated value of B_{BKW}. Typically this third component is calculated by determining the equivalent linear damping from experimental data and then subtracting the other damping values.

5.1 Frictional Damping

To calculate the first component B_F, the skin friction laws for a flat plate in a steady flow are applied to the roll motion of the body. Kato [13] demonstrated this with his formula:

$$B_{F0} = 0.787\rho S r_s^2 \sqrt{\omega\nu}\{1 + 0.00814(\frac{r_s^2\phi_A^2\omega}{\nu})^{0.386}\} \tag{5.2}$$

where ρ represents density, ω is the frequency, ν is the kinematic viscosity of the fluid, ϕ_A is the roll amplitude, S represents the wetted surface area of the ship, and r_s is the average radius of roll. S and r_s are calculated as follows [11]:

$$S = L(1.7d + C_B B) \tag{5.3}$$

$$r_s = \frac{1}{\pi}\{(0.887 + 0.145C_B)\frac{S}{L} - 2\,OG\} \tag{5.4}$$

where L, d, C_B and B are the length, draft, beam, and block coefficient of the model, respectively. OG is defined as the vertical distance from the origin to the center of gravity. Then, from Himeno [11] B_F can be expressed as:

$$B_F = B_{F0}(1 + 4.1\frac{U}{\omega L}) \tag{5.5}$$

where U is the forward speed of the ship. For the model in consideration, the B_F is 0.1608 N m s. To confirm the accuracy of this frictional damping, first it must be nondimensionalized using Equation 5.6 [11].

$$\hat{B}_F = \frac{B_F}{\rho \nabla B^2}\sqrt{\frac{B}{2g}} \tag{5.6}$$

This results in a $\hat{B}_F$ value of 5.4907e-04 confirmed to be correct by Figure 4.1 in Himeno's work [11] which plots the values of $\hat{B}_F$ versus the Froude number. These $\hat{B}_F$ values are obtained from various different practical and theoretical tests, including Kato's [13] formulation (Equation 5.5) used in this thesis.

5.2 Lift Damping

With confirmation that this method works and is applicable to the model, the next component to be calculated is the lift damping B_L which is produced due to the forward speed of the ship. Figure 4.16 in Himeno's work [11] shows that lift damping is linearly related to the forward speed. B_L can be calculate using Equation 5.7 [11]:

$$B_L = \frac{\rho}{2} U L d k_N l_0 l_R [1 - 1.4\frac{OG}{l_R} + \frac{0.7\,OG}{l_0 l_R}] \tag{5.7}$$

where k_N is the derivative of the lift coefficient of the hull with respect to time when the hull is towed obliquely, and l_0 is defined so that the quantity $l_0\dot{\phi}/U$ represents the incidence

angle of the lifting body while l_R serves as the distance from point O to the center of the lift force [11]. To calculate k_N here, Yumuro *et al.*'s [26] formulation may be used as follows:

$$k_N = 2\pi\frac{d}{L} + \kappa(4.1\frac{B}{L} - 0.045) \tag{5.8}$$

where

$$\kappa = \left\{ \begin{array}{lll} 0 & & c_m \leq 0.92 \\ 0.1 & for & 0.92 < c_m \leq 0.97 \\ 0.3 & & 0.97 < c_m \leq 0.99 \end{array} \right\} \tag{5.9}$$

The l_0 and l_R values for this ship are as follows:

$$l_0 = 0.3d \tag{5.10}$$

$$l_R = 0.5d \tag{5.11}$$

This results in a B_L value of 0.7997 N m s. When nondimensionalized using Equation 5.12 [11] this results in a $\hat{B}_F$ value of 0.0027 which is confirmed to be correct from Figure 4.5 in Himeno's work [11]. The other components of damping can also be confirmed to be correct in the same way however this will not be shown in this paper. A confirmation on the final value of B_e will however be done to ensure accuracy.

$$\hat{B}_L = \frac{B_L}{\rho\nabla B^2}\sqrt{\frac{B}{2g}} \tag{5.12}$$

When looking at Figure 4.5 in Himeno's work to ensure accuracy, it is important to realize that at a Froude number of 0.2, B_E (and therefore $\hat{B}_E$) is equal to 0. This can be confirmed

from Figure 4.16 in Himeno's work [11]. It should also be noted that due to a large spread in the data at each Froude number, and the low resolution of the y-axis, the $\hat{B}_L$ can only be approximated from the graph. However this resolution was deemed to be enough to confirm the values obtained from Equation 5.7 by Ikeda *et al.* [12].

5.3 Wave Damping

The next component of B_e is wave damping, B_W. B_W represents the increase in hull-pressure damping due to the presence of free surface waves. The interactions between waves and eddies as well as between waves and lift are accounted for here. However, since these elements are typically very small, B_W is generally linear as seen in Figure 4.16 in Himeno's work [11]. Ikeda *et al.* [12] constructed an empirical formula for B_W by calculating the energy loss between a pair of horizontal doublets and adding those results to experimental data from combined flat plates. This gave rise to Equation 5.13 [12] to approximate the wave damping component of the ship

$$\frac{B_W}{B_{W0}} = 0.5[\{(A_2+1)+(A_2-1)tanh(20\tau-b)\}+(2A_1-A_2-1)exp\{-150(\tau-0.25)^2\}] \quad (5.13)$$

where

$$A_1 = 1 + \xi_d^{-1.2} e^{-2\xi_d} \quad (5.14)$$

$$A_2 = 0.5 + \xi_d^{-1} e^{-2\xi_d} \quad (5.15)$$

$$\xi_d = \omega^2 d/g \tag{5.16}$$

$$\tau = U\omega/g \tag{5.17}$$

B_{W0} is the case where the Froude number is zero and can be obtained using the strip method as follows [11]:

$$B_{W0} = \rho N_S (l_w - OG)^2 \tag{5.18}$$

This resulted in a B_W value of 0.7254 N m s for this ship.

5.4 Normal Force Damping of Bilge Keels

Next, the damping due to the different forces on a pair of bilge keels must be dealt with. It is important to remember that this includes damping due to the bilge keels themselves as well as the added damping due to the interactions between the bilge keels, the hull, and the waves. Through much of the previous work done in the field of naval architecture it can be concluded that bilge keel damping is driven largely by roll amplitude and frequency, and can be observed in [11]. This can also be viewed in Figure 4.16 in Himeno's work [11] where the different bilge keel dampings do not seem to change drastically with increasing ship speeds.

The dimensions for the bilge keel added to the model are presented in Table 3.1. The l_{BK} term represents the length of the bilge keel while the b_{BK} is the width of the bilge keel.

The first component of this damping term is the Normal-force damping of bilge keels, which,

as the name suggests, is due to the normal force on the bilge keels. Starting with the definition for coefficient of drag on the bilge keel, Ikeda *et al.* [12] developed the following to calculate B_{BKN}:

$$B_{BKN} = \frac{8}{3\pi}\rho r^2 b_{BK}^2 \omega f^2 \{\frac{22.5}{\pi f} + 2.40\frac{r\phi - A}{b_{BK}}\} \tag{5.19}$$

where f is an empirical coefficient of velocity increment and calculated by Equation 5.20 [12]. The σ represents the area coefficient of the ship hull section.

$$f = 1 + 0.3exp\{-160(1-\sigma)\} \tag{5.20}$$

Fujino *et al.* [7] took a different approach to solving the Normal force damping of bilge keels however their solution also confirmed the validity of Ikeda's solution. Equation 5.19 results in a B_{BKN} value of 1.042 N m s.

5.5 Hull Pressure Damping due to Bilge Keels

The last component that needs to be considered at a Froude number of 0.2 for the ship in question is the hull pressure damping due to bilge keels B_{BKH}. This component of damping arises from the pressure change on the hull from the installation of the bilge keels [11]. Ikeda *et al.* [12] as well as Goda and Miyamoto [9], with some assumption on the C_P distribution determined a formulation for B_{BKH} as follows:

$$B_{BKH} = \frac{4}{3\pi}\rho r^2 d^2 \omega \phi_A f^2 I \tag{5.21}$$

where

$$I = \frac{1}{d^2} \int C_P \, l_0 \, ds \tag{5.22}$$

This results in a B_{BKH} value of 0.9581 N m s.

5.6 Equivalent Linear Damping

With the different components of the equivalent linear damping now known, it is possible to calculate B_e using Equation 5.1. The values are shown in Table 5.1:

Table 5.1: Summation of different components of damping

Components	**Value (N m s)**
B_F	0.1608
$B_F + B_L$	0.9605
$B_F + B_L + B_W$	1.6859
$B_F + B_L + B_W + B_{BKN}$	2.7279
$B_e = B_F + B_L + B_W + B_{BKN} + B_{BKH}$	3.6860

To confirm that the final value of the equivalent linear damping is accurate, it must first be nondimensionalized just like the other damping components using Equation 5.23 [11].

$$\hat{B}_e = \frac{B_e}{\rho \nabla B^2} \sqrt{\frac{B}{2g}} \tag{5.23}$$

This results in a $\hat{B}_e$ value of 0.0126. This $\hat{B}_e$ value is confirmed to be correct from Figure 5.4 in Himeno [11] at a Froude number of 0.2. The nondimensionalized value for the equivalent linear damping without the bilge keels is 0.0058 from an Equation similar to Equation 5.23. This too is confirmed to be accurate from Figure 5.4 in Himeno [11].

Now that the values of the different components of the linear equivalent damping are known there was a desire to learn if FDEs could be used to represent them. It was theorized that some relationship might be found between the a and b coefficients (Equation 3.3) and the damping components. This was accomplished through the Matlab program developed and verified earlier. The results for two of these five cases are shown here: Just the B_F component and the final linear equivalent damping B_e. The other cases follow a similar pattern and are included in the Appendix. The B_F case shown in Figure A.1 was chosen in particular since it has the highest error and slightly different a and b values. The B_e case in Figure 5.2 demonstrates the final output and depicts the result at a high damping coefficient.

The resulting values for coefficients a and b are presented in Table 5.2. The coefficients are plotted against damping in Figure 5.3 and Figure 5.4 respectively. It is evident from these figures that there is a relation between the value of the coefficients and that of the damping. This will be further investigated in the next chapter.

Table 5.2: Values of the damping components added up with the corresponding a and b values

Component	**Value**	**Corresponding** a	**Corresponding** b
B_F	0.1608	1.4184	0.651
$B_F + B_L$	0.9605	1.1082	1.1
$B_F + B_L + B_W$	1.6859	1.0694	1.8
$B_F + B_L + B_W + B_{BKN}$	2.7279	1.0306	2.8
$B_e = B_F + B_L + B_W + B_{BKN} + B_{BKH}$	3.686	1.0306	3.7

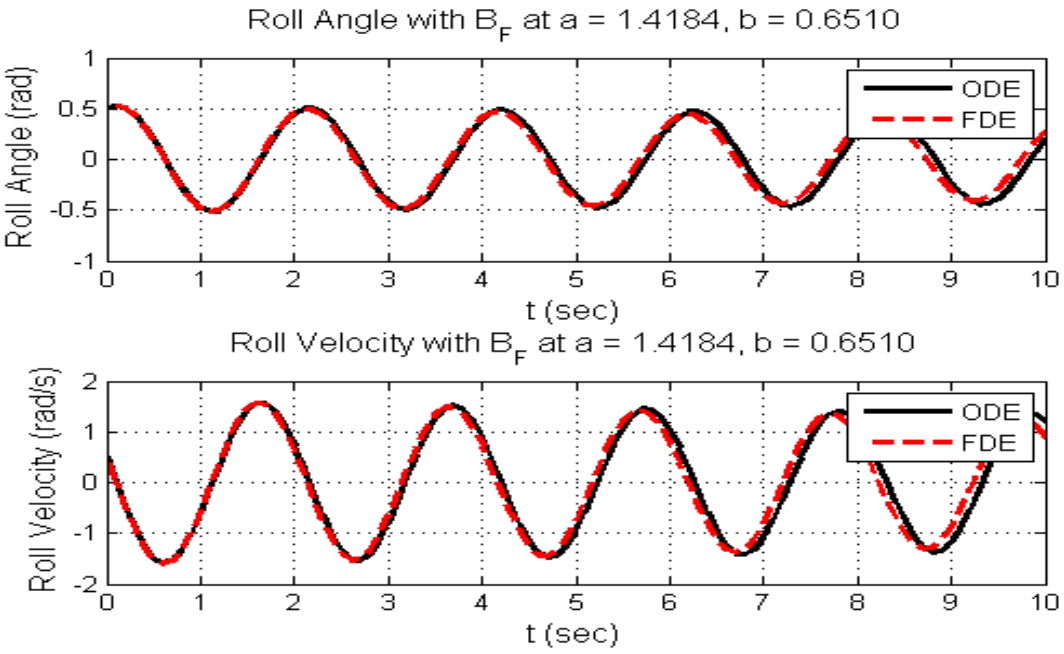

Figure 5.1: Roll angle and roll velocity vs. time when damping = B_F

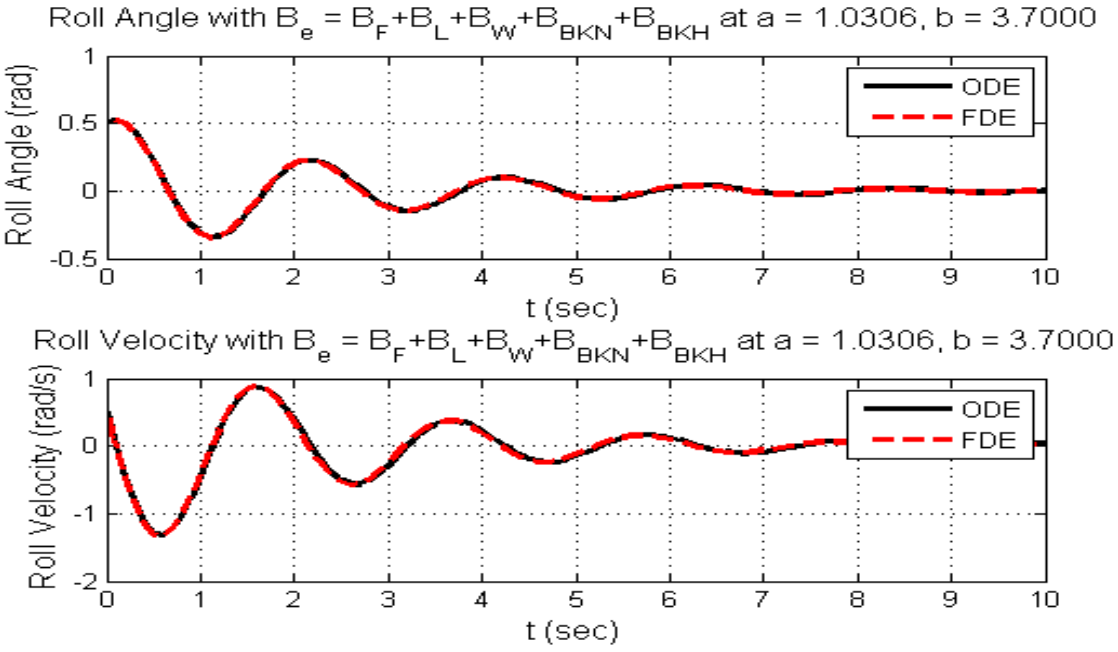

Figure 5.2: Roll angle and roll velocity vs. time when damping = B_e

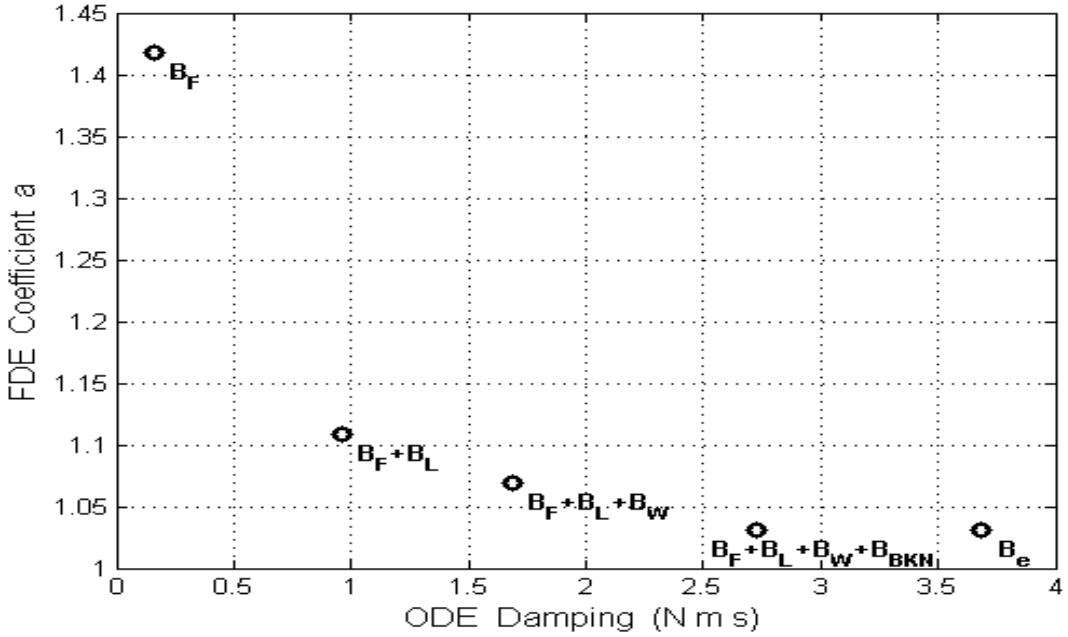

Figure 5.3: Values of coefficient a vs. damping

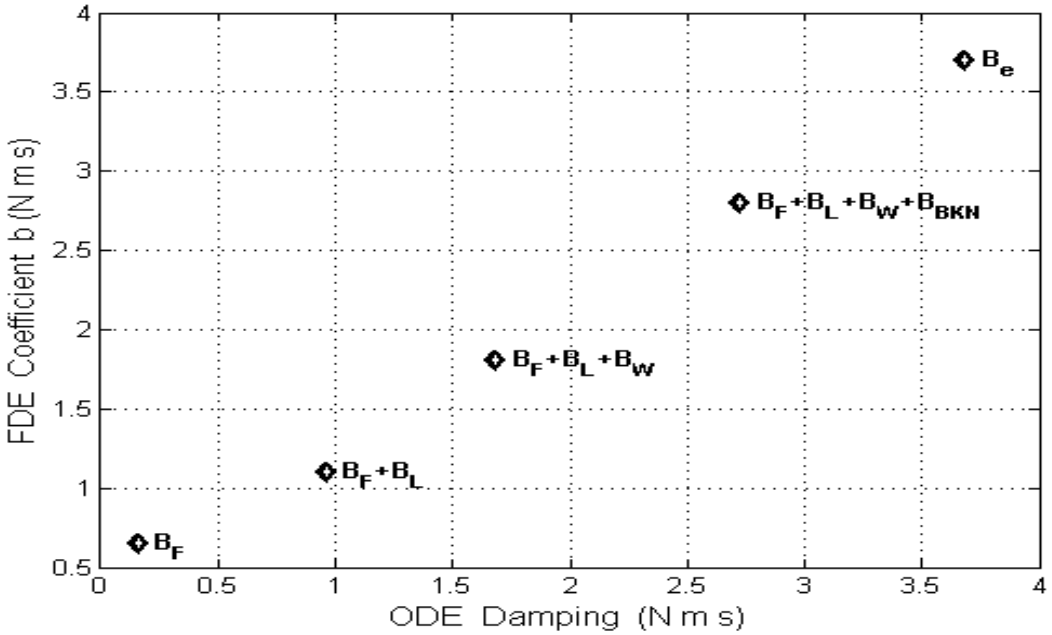

Figure 5.4: Values of coefficient b vs. damping

Chapter 6

Further Investigation of Roll Damping

6.1 Varying the ODE Damping

To determine a trend between the FDE coefficients and the ODE damping value, a sweep was conducted over a range of ODE damping values. The range of this sweep was from a damping value of 0.1 N m s to 7.0 N m s. The optimal a and b values and the corresponding error were calculated at each of these damping values. The results are displayed in Figures 6.1 - 6.3. No individual runs were presented here since examples of similar runs can be found in Chapter 5.

Figure 6.1 depicts that the coefficient a approaches a constant value as the ODE damping increases. In the scenario run here, this a value was 1.0306. Figure 6.2 shows that at higher damping values, the FDE model tends toward the ODE model, likely because the damping, rather than the added inertia effects, drive the dynamics. Figure 6.3 illustrates that as the ODE damping increases, the error decreases. This is invaluable information since all the conclusions that can be drawn from Figures 6.1 and 6.2 are at the higher damping values.

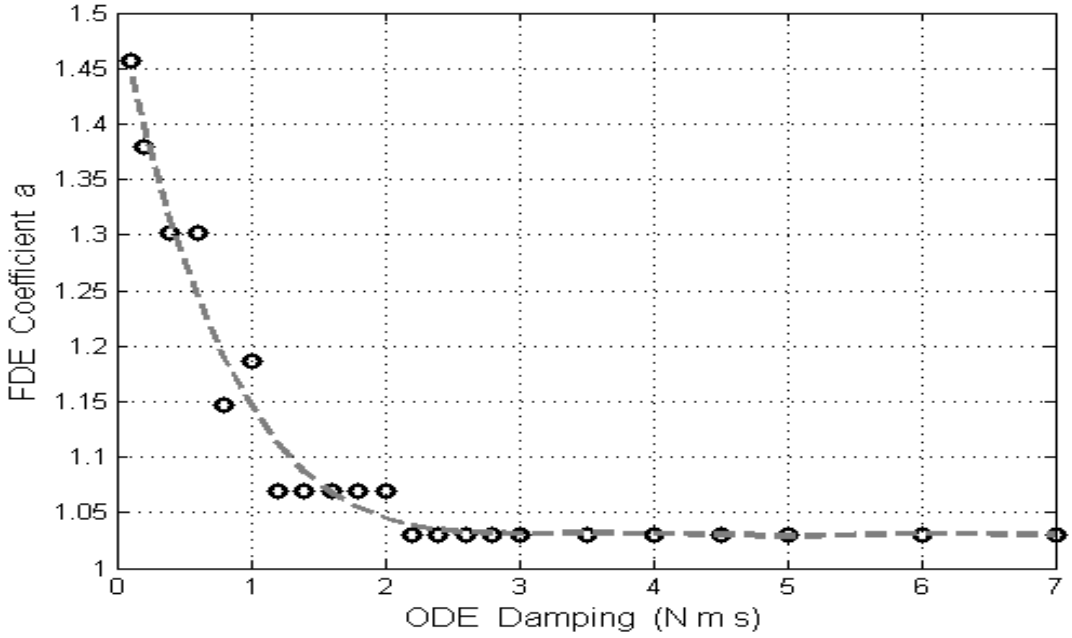

Figure 6.1: Coefficient a vs. ODE Damping (N m s)

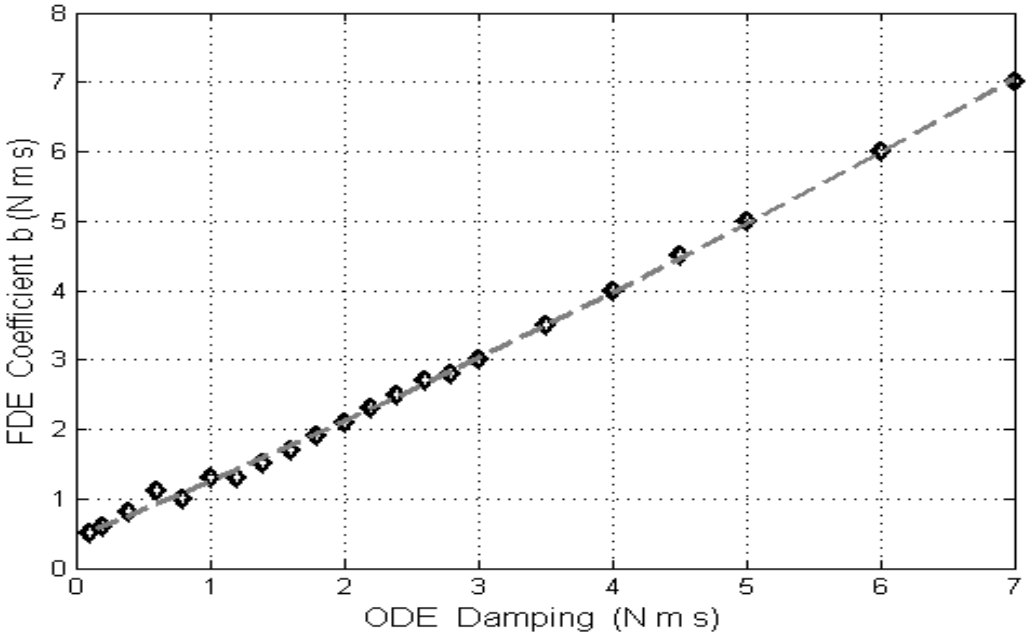

Figure 6.2: Coefficient b (N m s) vs. ODE Damping (N m s)

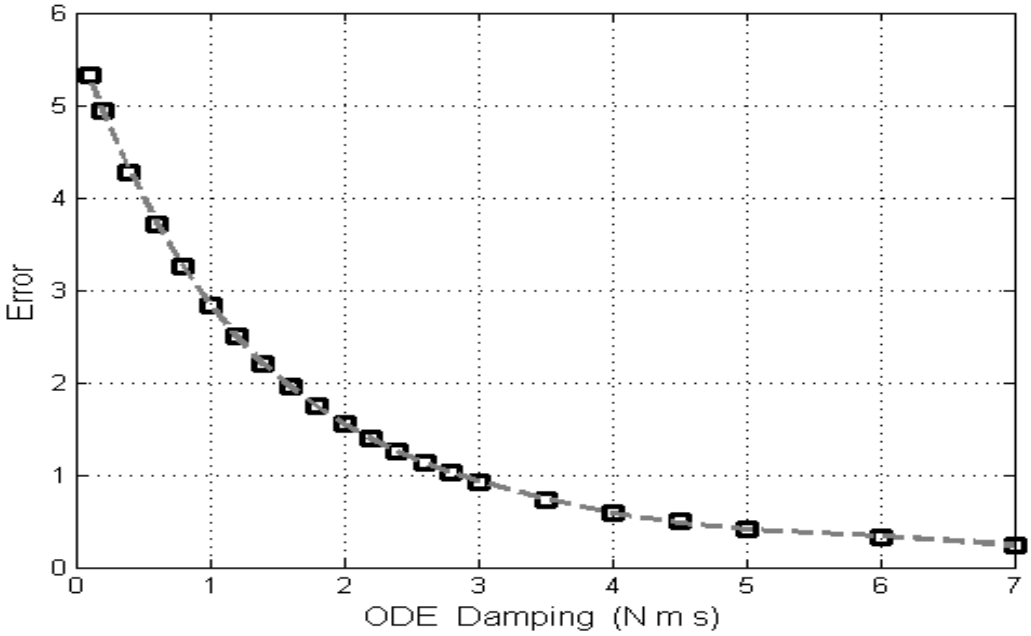

Figure 6.3: Error vs. ODE Damping (N m s)

6.2 Varying the Added Moment of Inertia

To determine a relationship between the a, b, and error values and the added moment of inertia δI, the ODE damping value was held constant at 1.4 N m s. A sweep of δI values ranging from 0.01 kg m^2 to 1 kg m^2 was carried out and the resulting optimal a and b values and the corresponding error were graphed in Figure 6.8. Figures 6.4 and 6.6 present the roll angle and roll velocity versus time for a δI of 0.01 kg m^2 and 1 kg m^2 respectively. These are the two extremes of the range of δI values considered here. It can be clearly seen from these plots that the FDE tracking depreciates considerably with increasing added moment of inertia. However it should be noted that the δI for this model is 0.0973 kg m^2 so at some point this δI is no longer physically relevant. Figures 6.5 and 6.7 demonstrate how the amount of error and the uncertainty increases when the added moment of inertia increases.

Figure 6.8 is a concise visual representation of the behavior of coefficients a and b and the error with increasing δI. The value of a remains fairly constant starting at a value of 1.1 and ending at a value of approximately 1.4. However the value of b increases steadily to compensate for the increasing δI. The error is also consistently getting larger with higher δI values.

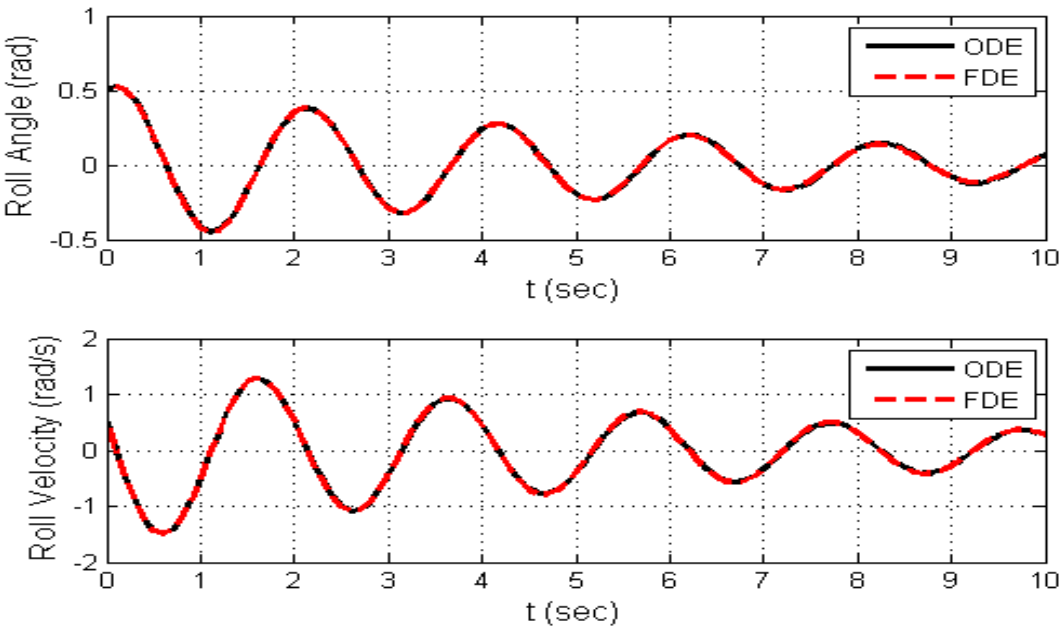

Figure 6.4: Roll angle and roll velocity vs. time when δI = 0.01 kg m^2

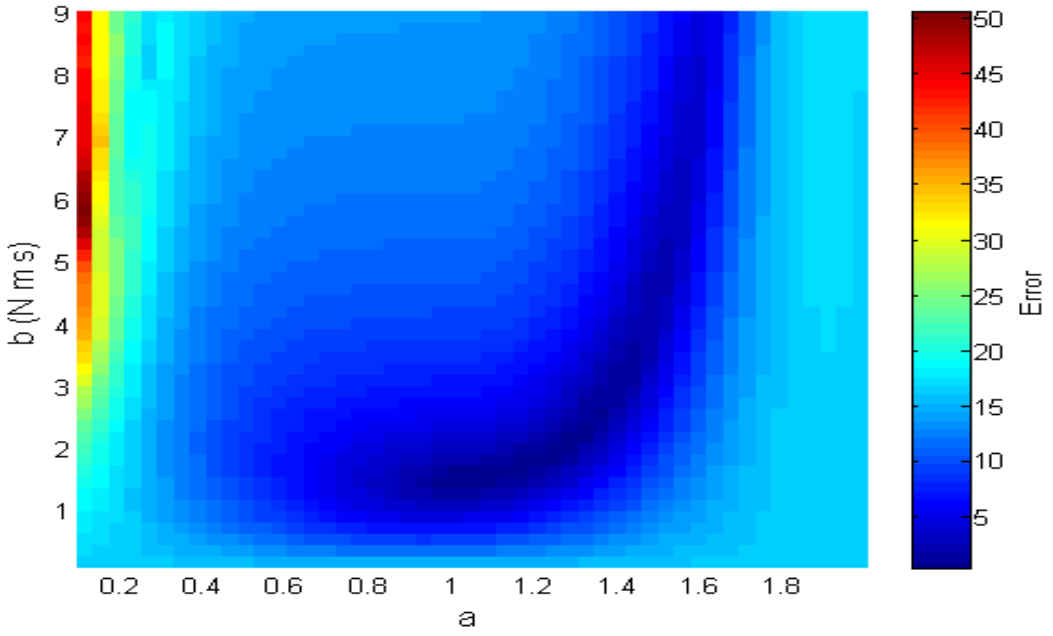

Figure 6.5: Error in roll angle and roll velocity at different numeric values of a and b when δI = 0.01 kg m^2

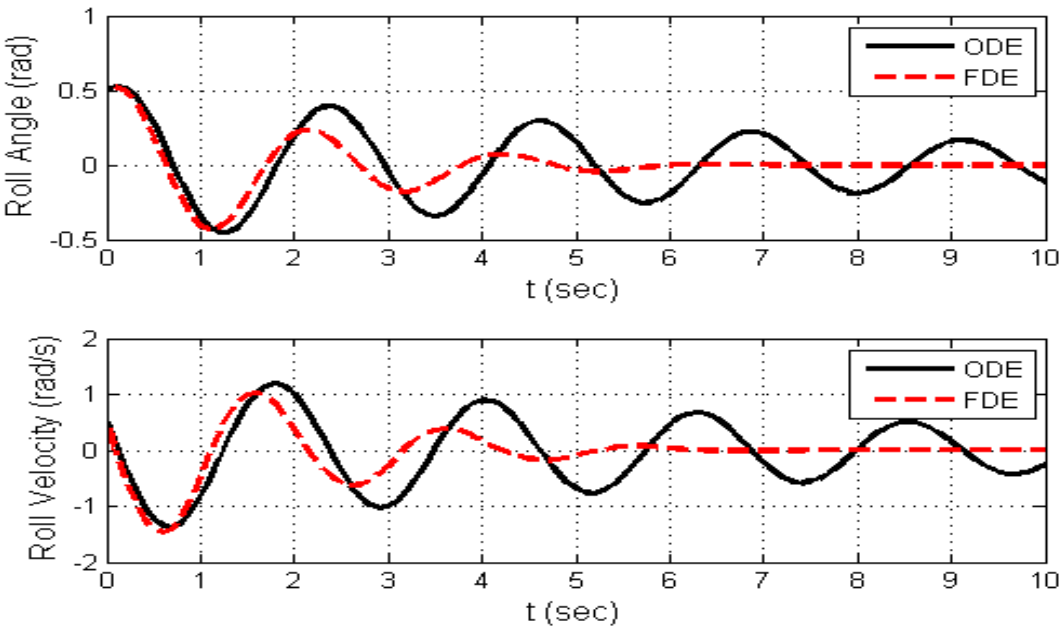

Figure 6.6: Roll angle and roll velocity vs. time when δI = 1 kg m^2

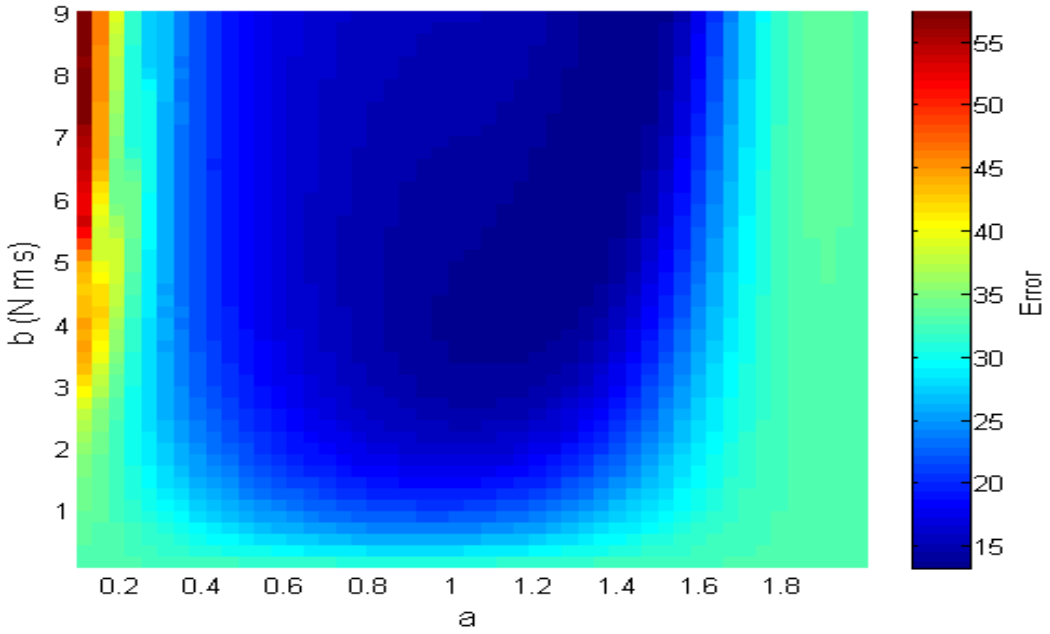

Figure 6.7: Error in roll angle and roll velocity at different numeric values of a and b when δI = 1 kg m^2

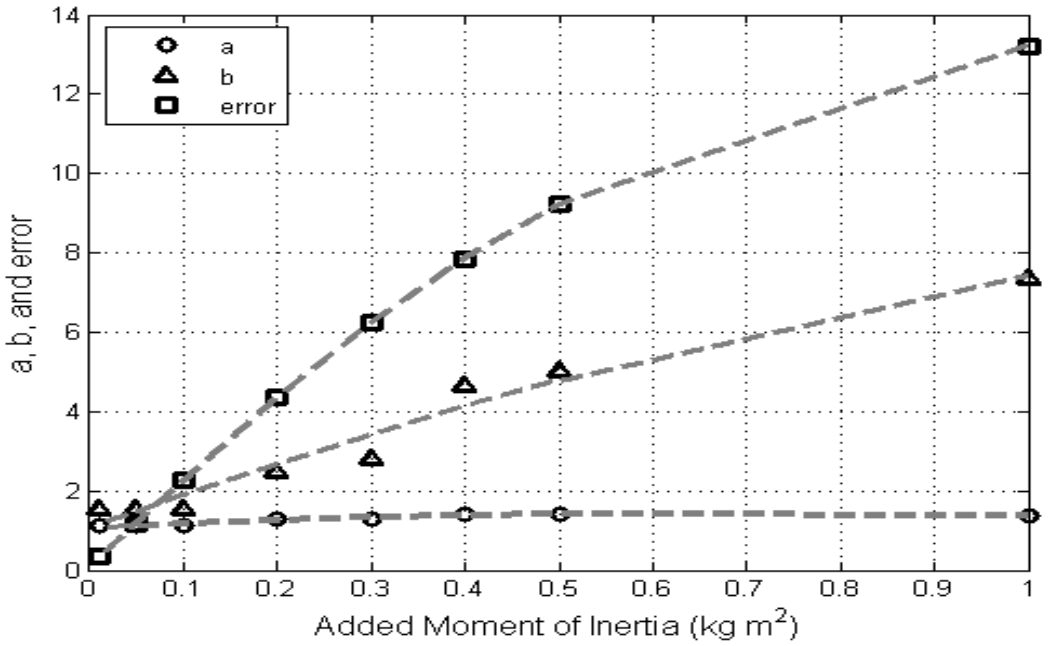

Figure 6.8: a, b, and error values vs. the added moment of inertia (kg m^2)

6.3 Varying the Initial Roll Angle

To understand how the initial condition for the roll angle ϕ may affect values of a, b and the error, ten cases were run spanning ϕ values from 0.1 to 1 radian. The values of the initial roll velocity $\dot{\phi}$ and the ODE damping were kept constant at 0.5 radians/s and 1.4 N m s respectively.

Using a similar presentation to that utilized when studying δI, Figures 6.10 and 6.12 depict the roll angle and roll velocity at the two extreme starting conditions considered: 0.1 radians and 1 radian. Despite both of these graphs starting at different initial conditions, it is hard to tell any difference in the quality of FDE tracking from visual inspection. Figures 6.11 and 6.13 however make it clear that a smaller starting condition has an overall smaller error and much less uncertainty than at larger ϕ_0.

Figure 6.9 is a presentation of the a, b, and error values at every starting roll angle considered.

the value of the coefficient a remains fairly constant through out starting and ending at values of 1.05 and 1.2 respectively. Similarly, b remains fairly constant at approximately 1.5 N m s before jumping to 2.1 N m s at a starting roll angle of 1 radian. However this is not a large cause for concern since the roll angle is starting to get substantial and possibly approaching the linear equivalent of the angle of vanishing stability. The error increases linearly with the initial condition leading to the conclusion that FDEs can track ODEs better at smaller angles. Despite this it should be noted that the error even near the angle of vanishing stability is still much smaller than the error due to larger δI values (Figure 6.8) or lower ODE damping values (Figure 6.3). Meaning that depending on the conditions, a larger starting condition is probably a smaller part of the total error when compared to the other variables.

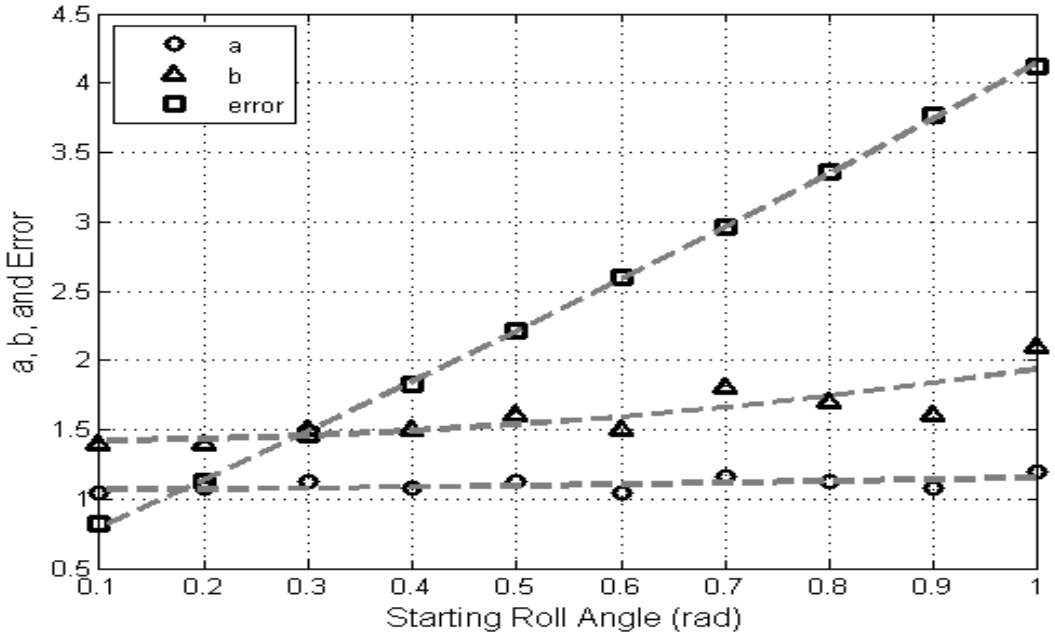

Figure 6.9: a, b, and error values vs. the starting roll angle (rad)

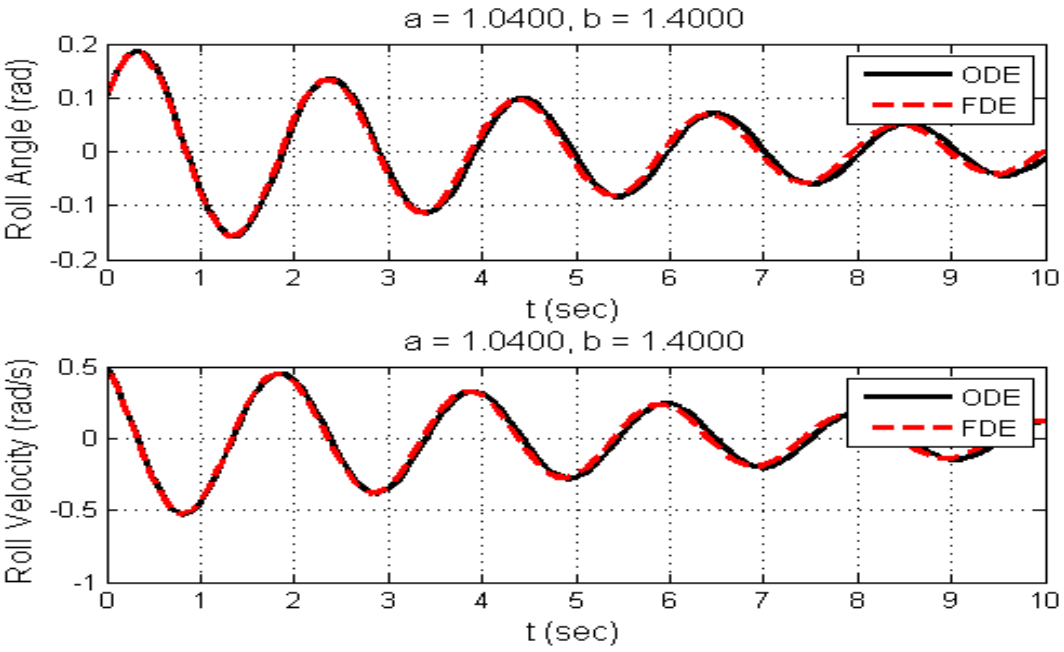

Figure 6.10: Roll angle and roll velocity vs. time when $\phi_0 = 0.1$ radian

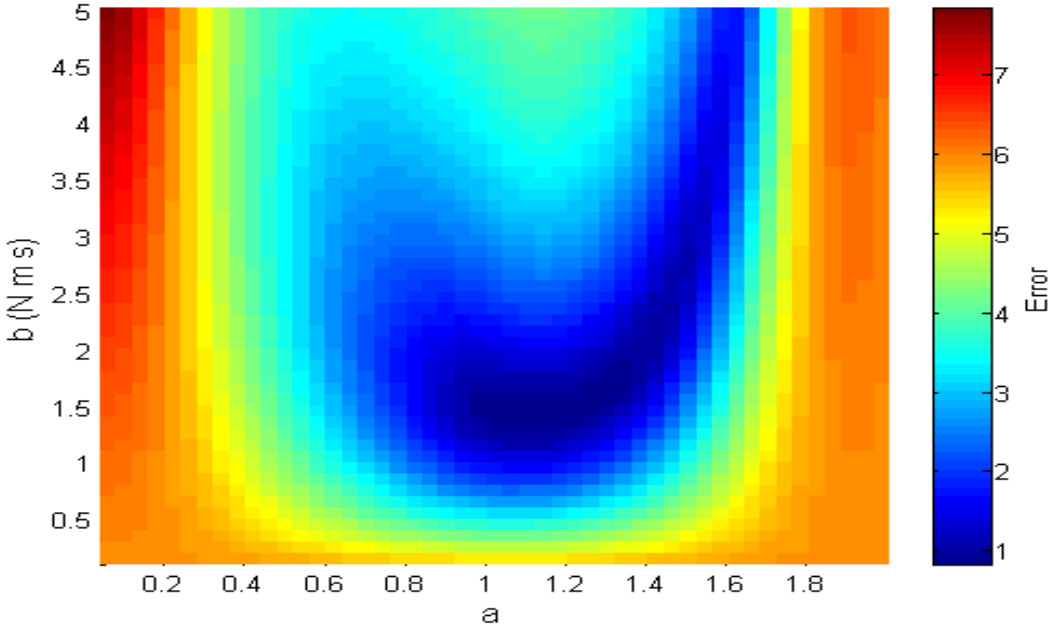

Figure 6.11: Error in roll angle and roll velocity at different numeric values of a and b when $\phi_0 = 0.1$ radian

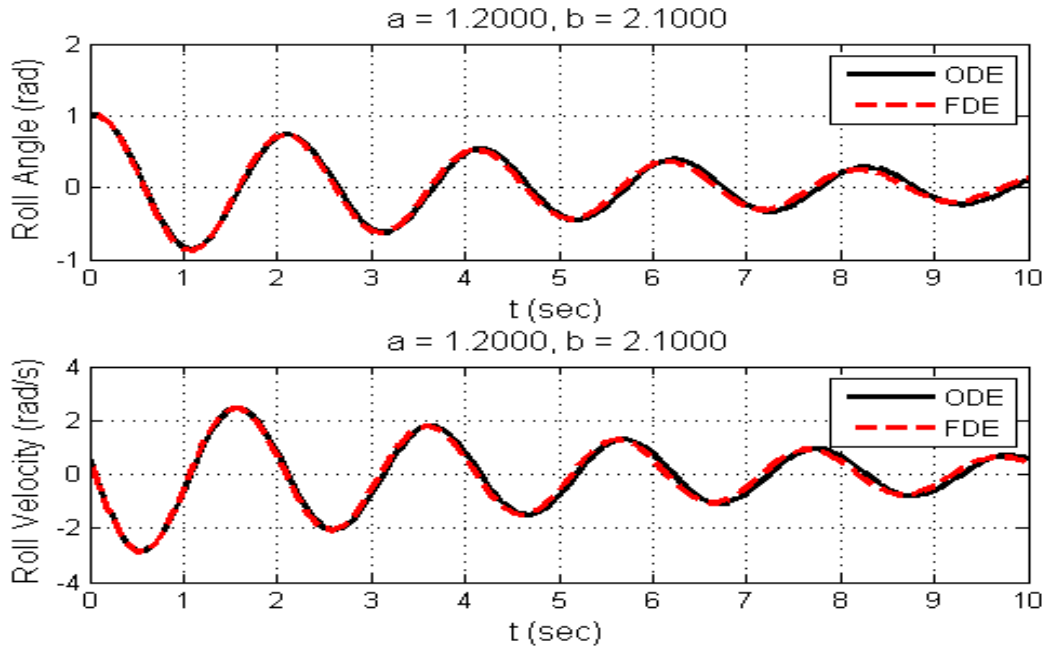

Figure 6.12: Roll angle and roll velocity vs. time when $\phi_0 = 1$ radian

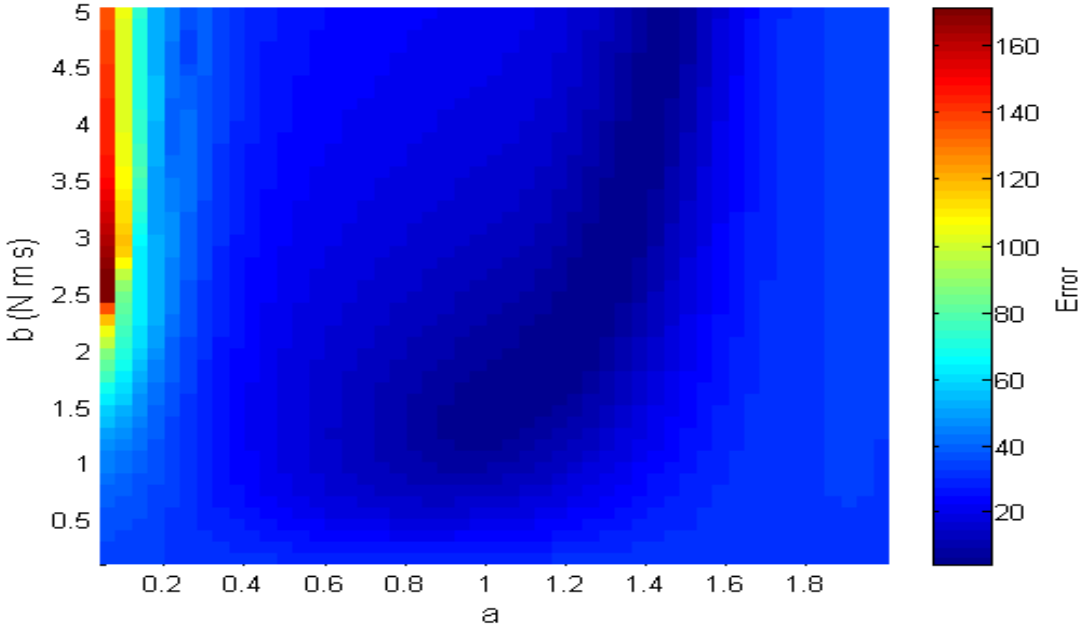

Figure 6.13: Error in roll angle and roll velocity at different numeric values of a and b when $\phi_0 = 1$ radian

Chapter 7

Roll vs. Pitch

Results from Chapter 6 raised questions as to how well a pitch model can be tracked by FDEs. Since higher damping results in lower error, and pitching would typically have large damping values it could be hypothesized that FDEs would be able to track a pitching model with greater accuracy. However, it was also shown that a higher δI results in higher error and a pitch model would have a substantially higher δI than the roll model decreasing its accuracy. Also yet unknown is the effect a larger moment of inertia I and metacentric height GM_L would have on the accuracy of the FDE model. With this in mind, the pitch model was set up using Equations 3.5-3.8. Substituting the new values into Equations 3.2 and 3.3 results in the pitch model. For this model the initial conditions for pitch angle and pitch velocity are both set to a constant 0.5 radians and 0.5 radians/sec respectively. The added mass moment of inertia δI is 0.4576 kg m^2.

To ensure that the new model and program are still functioning as desired, another check similar to Chapter 4 is performed here at a ODE damping of 1.5 N m s. The results shown in Figures 7.1 and 7.2 confirm the program picks an a value of 1, and b value of 1.5, and that the resulting error is 0.

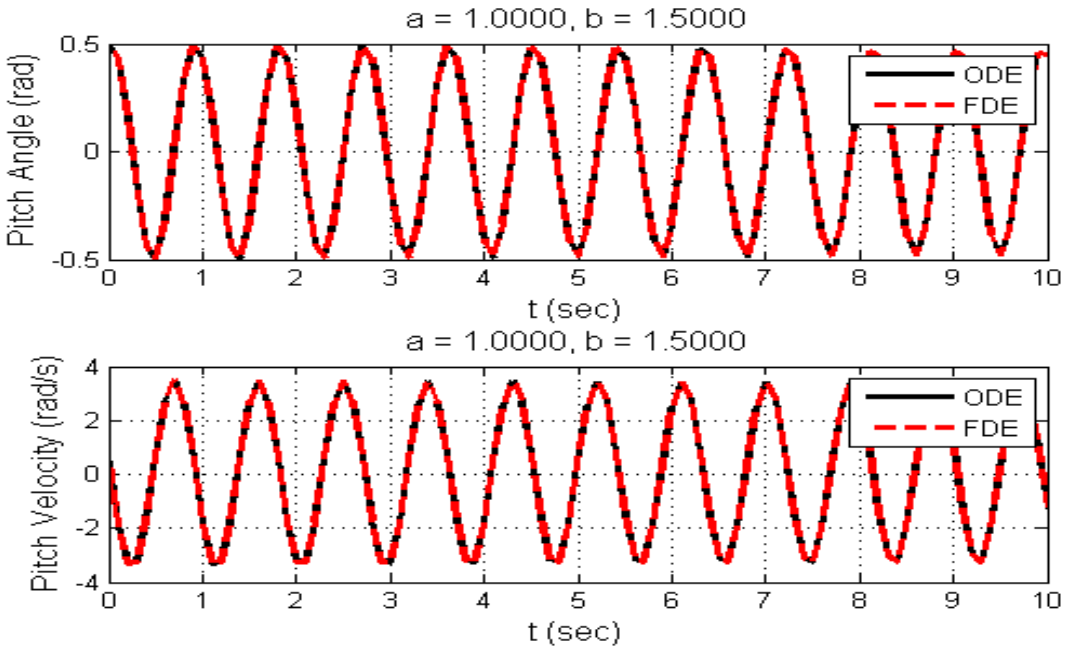

Figure 7.1: Pitch angle and pitch velocity vs. time when ODE damping = 1.5 N m s

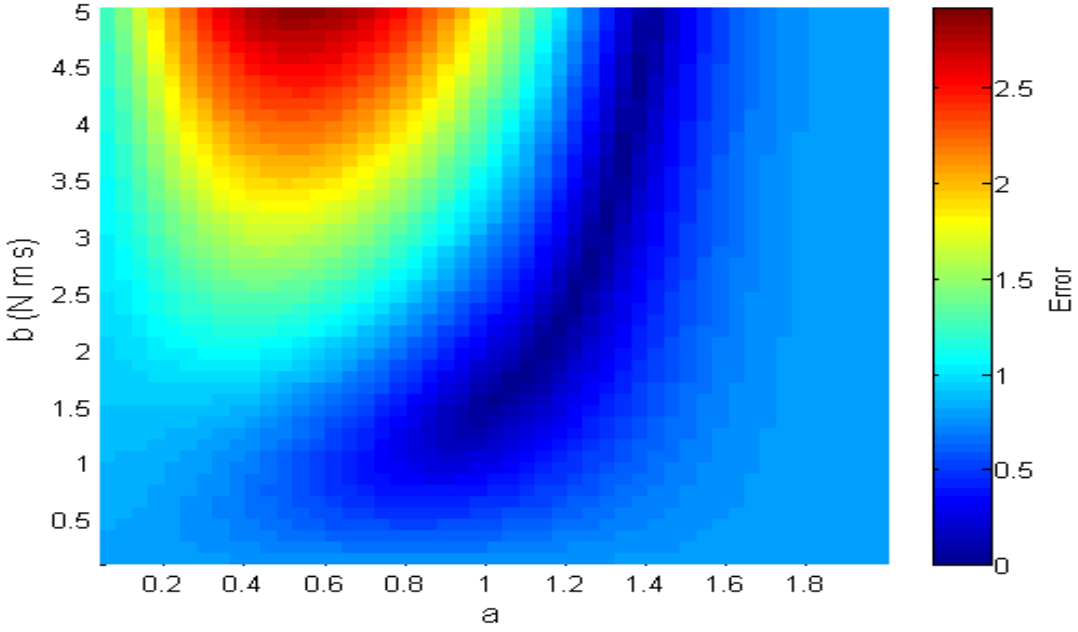

Figure 7.2: Error in pitch angle and pitch velocity at different numeric values of a and b when ODE damping = 1.5 N m s

With assurances that the program still performs as required with the new model, the optimization routine is run for a series of ODE damping values. An important note to make here is that the pitching model is analyzed on two different scales: roll-relevant damping and pitch-relevant damping. The roll-relevant scale looks at the behavior of the pitch model at ODE damping values appropriate for roll and compares the two results. The pitch-relevant scale on the other hand operates at higher ODE damping values appropriate for pitch and tries to capture the overall effect of increasing pitch damping.

Figures 7.3-7.5 present the results from the roll-relevant scale. Figure 7.3 compares the values of a for the roll and pitch models. Whereas the roll model presents systematic values of a with a clear trend apparent, the pitch model is still behaving as an FDE and cannot provide real meaningful conclusions. The same conclusion can be drawn from Figure 7.4 which compares the b value for the roll and pitch models. The value of b increases in both models, however the increase in the pitch model is erratic and it would be hard to confidently state the trend in the future. Neither of these conclusions should come as a surprise though since the roll dynamics are being driven by damping at this scale, whereas the pitch dynamics are still under the effects of the added inertia. Figure 7.5 is comparing the error between the pitch and roll models and presents an interesting situation. The error in the pitch model is lower than the roll model for ODE damping of less than 2 N m s. It is only after this ODE damping value, that the pitch model consistently has more error. However this conclusion too should be made with caution for this thesis chose to use time as the constant variable for comparison, and not the number of oscillations. Figures 7.6 and 7.7 demonstrate how this leads to a different number of oscillations being compared which could possibly lead to a higher error accumulating with increasing oscillations. A future area of study might be keeping the number of oscillations constant and comparing the two models under this new condition.

Figures 7.8-7.10 present the coefficients a, and b and the subsequent error for the pitch model on the pitch-relevant scale. Here, the trends visible in the previous chapter for the roll model start to appear again. Figure 7.8 details coefficient a returning to a value of 1 as the ODE damping increases. Figure 7.9 similarly shows coefficient b starting to equate the damping from the ODE model. Once again it would seem that the damping is starting to drive the FDE model. With the observation of these trends it is once again possible to draw future conclusions of this model without the need for running more cases. The error for the pitch model presented in Figure 7.10 can be seen to decay exponentially enabling greater accuracy for conclusions drawn in the future at large damping values.

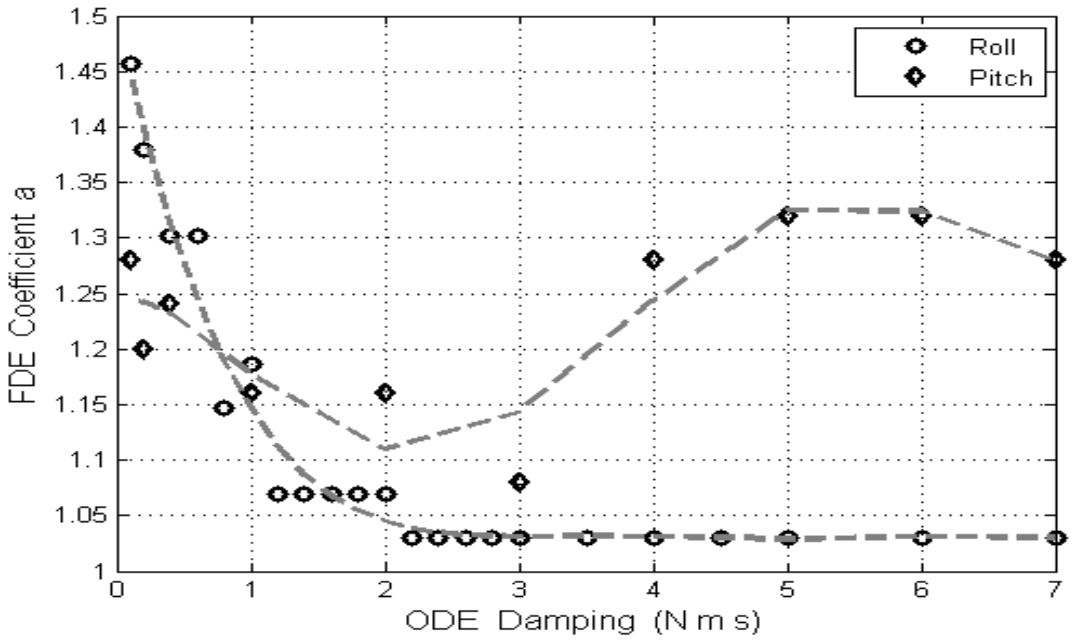

Figure 7.3: Coefficient a for roll and pitch models vs. ODE Damping (N m s)

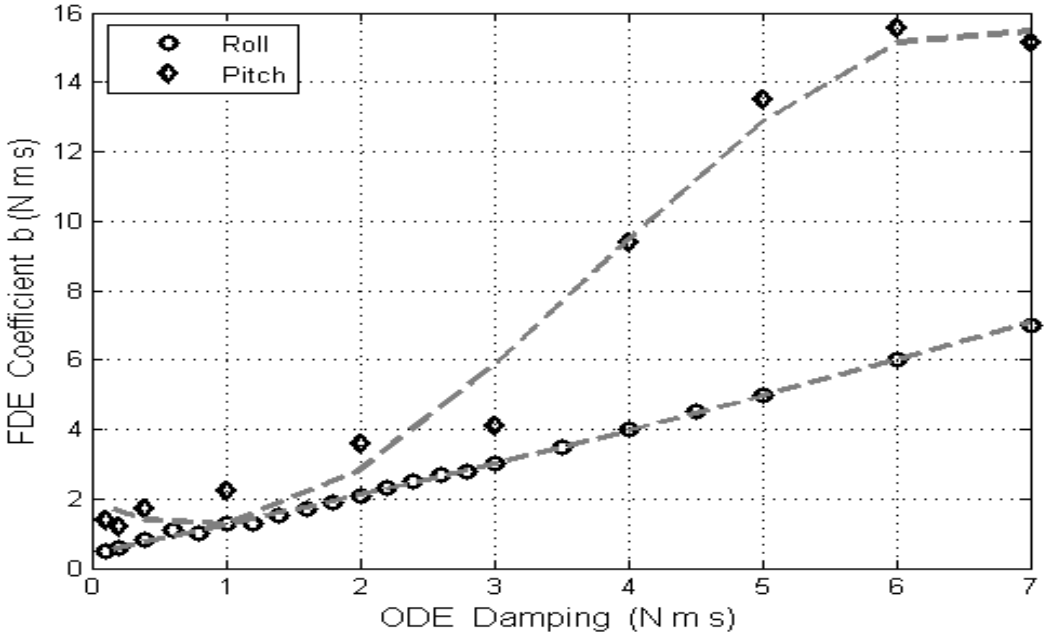

Figure 7.4: Coefficient b for roll and pitch models vs. ODE Damping (N m s)

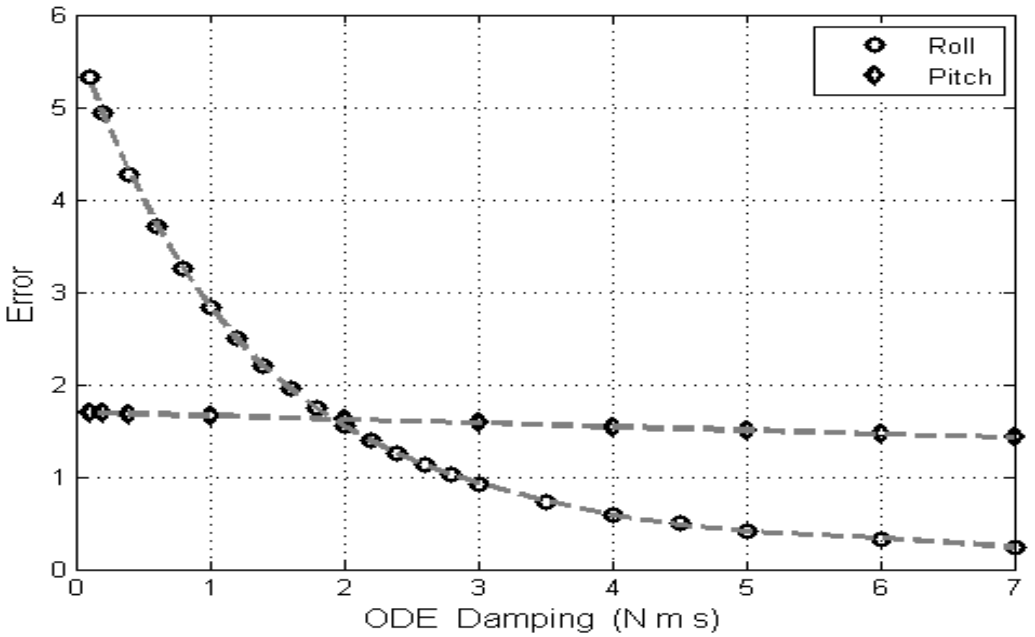

Figure 7.5: Error in the roll and pitch models vs. ODE Damping (N m s)

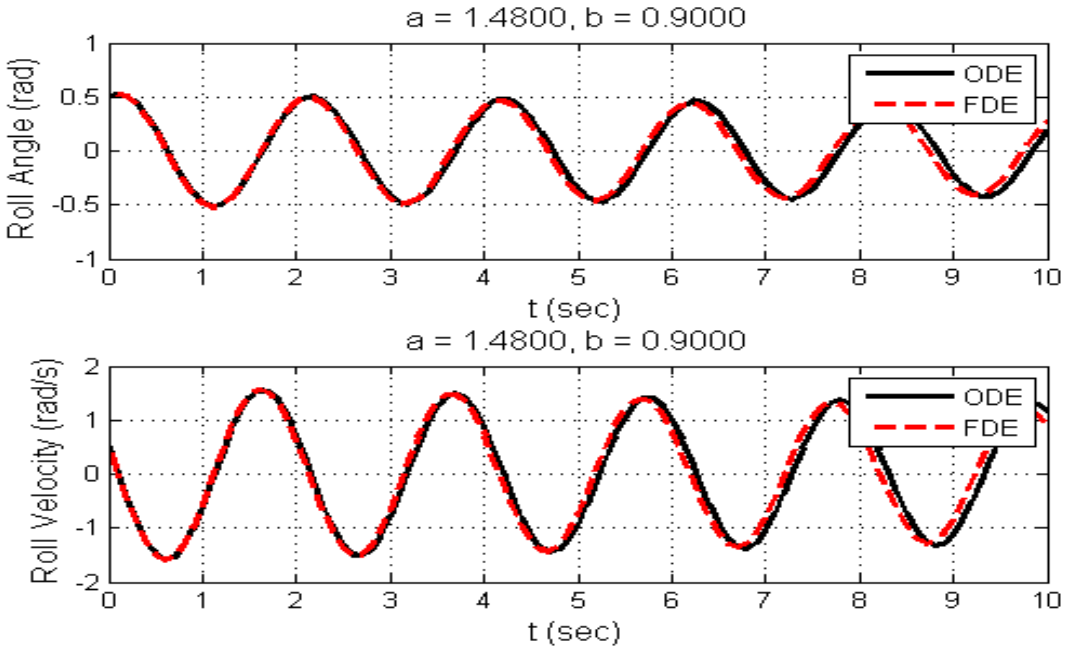

Figure 7.6: Roll angle and roll velocity vs. time when ODE damping = 0.2 N m s

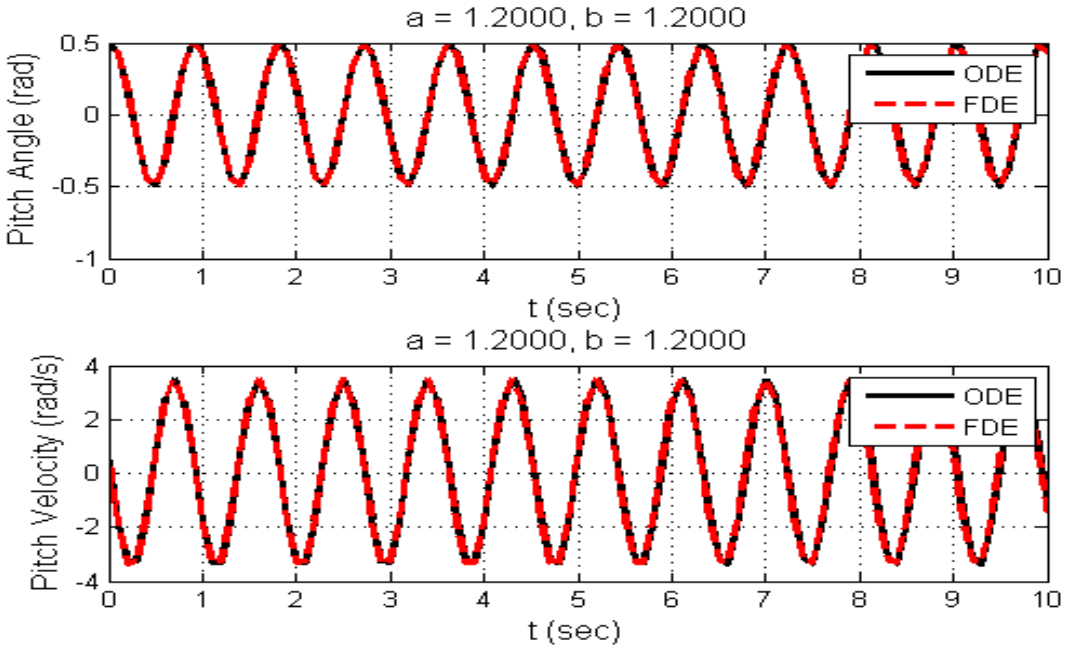

Figure 7.7: Pitch angle and pitch velocity vs. time when ODE damping = 0.2 N m s

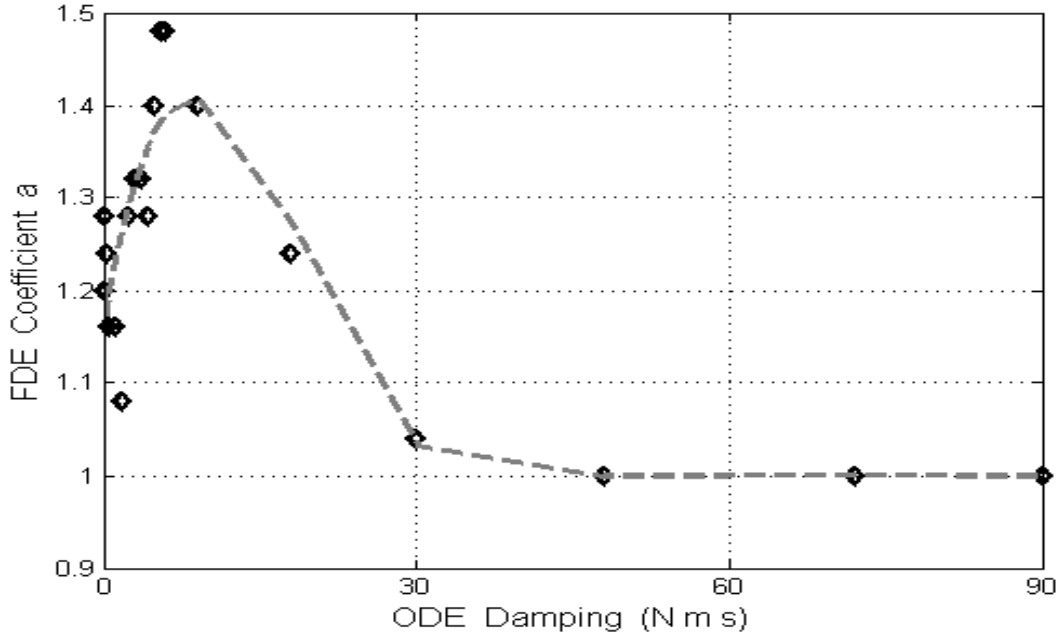

Figure 7.8: Coefficient a for the pitch model vs. ODE Damping (N m s)

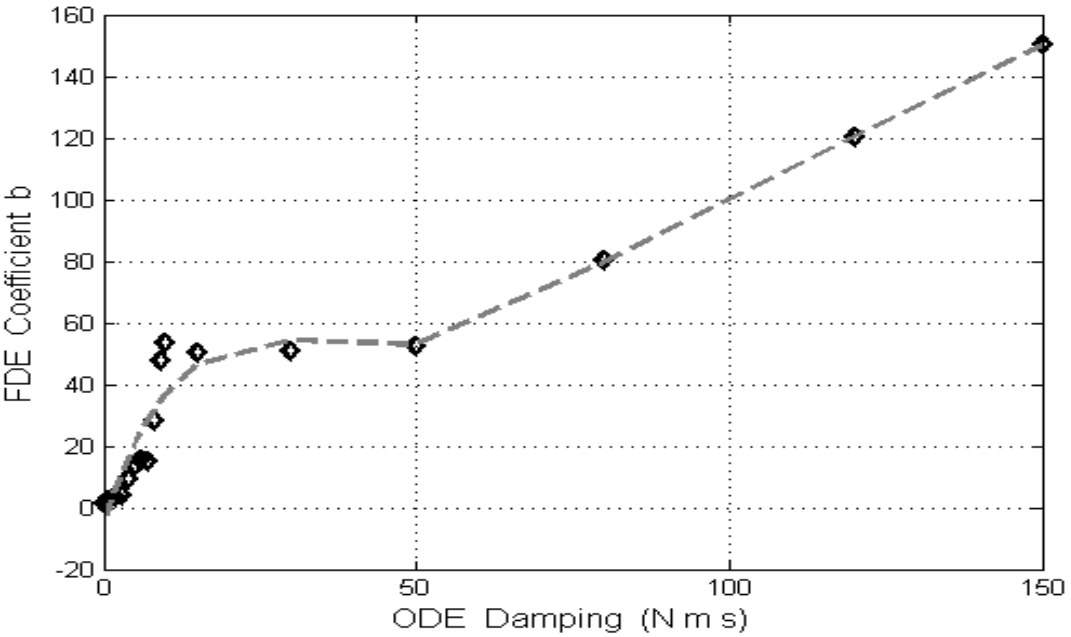

Figure 7.9: Coefficient b for the pitch model vs. ODE Damping (N m s)

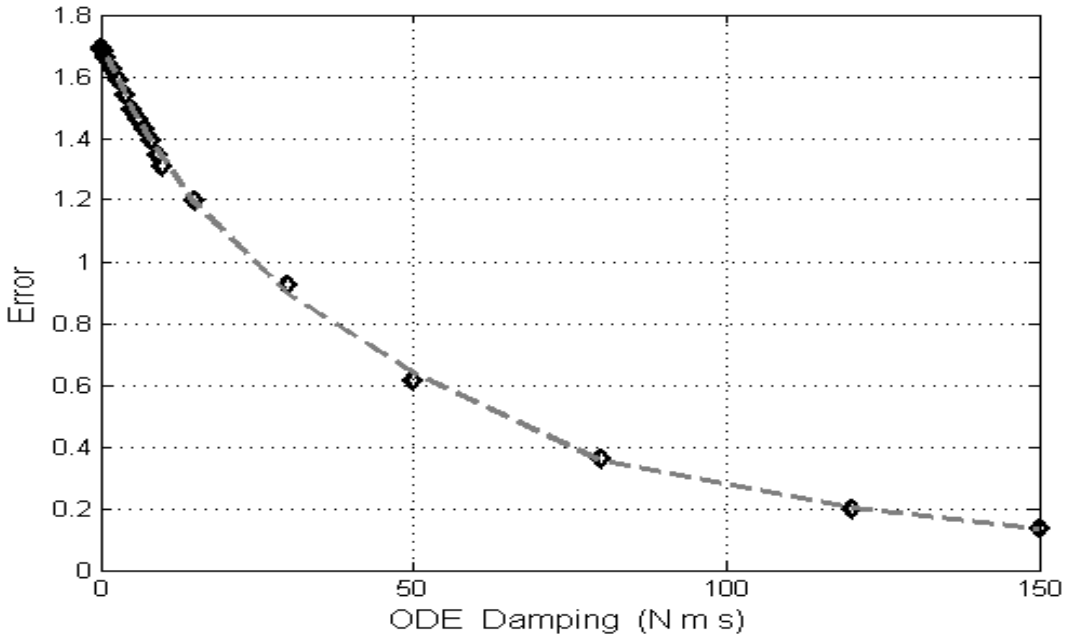

Figure 7.10: Error for the pitch model vs. ODE Damping (N m s)

Chapter 8

Summary

The algorithm in this thesis was developed for a simplified model dealing with single degree of freedom motion in an effort to further the state of knowledge on the influence of fractional differential equation order on the nature of roll damping. Euler's generalized approach was used to solve the FDEs. The goal of the code was to obtain the optimal a and b coefficients when compared to a similar ODE with added moment of inertia. The code uses Matlab built-in function **ode45** and was tested to ensure that it operates as required. It was then applied to a variety of roll models. A pitch model was also developed and compared to the roll model. The code was also tested against the different components of damping developed by Ikeda *et al.* [12] and Himeno [11].

8.1 Conclusion

The outputs from the code developed included coefficients a and b and the associated error. When these were applied to the roll motion, both Himeno's model and a general model, a variety of conclusions were drawn. It was shown that as the ODE damping value increases

the FDEs start being driven by the damping. With increasing ODE damping the value of a starts to approach 1 and b starts to equate to the ODE damping. Effectively the FDE transforms into the ODE. The error also decreases as the ODE damping increases. This is probably because at these larger damping values the FDE practically resembles the ODE thus driving the error to 0. Table 5.2 depicts this trend with the various components of damping from Himeno's work.

The derived pitching model yielded the following conclusions: If a comparison is done between the roll and pitch model with time (and not the number of oscillations) being constant, the FDE is better at tracking pitch for ODE damping values less than 2 N m s. After this the roll model has lower error and therefore better tracking. Also, if the pitch model is studied at damping values appropriate to such a model it behaves the same way as the roll model. At roll-relevant damping values however the pitch model does not have a clear trend and offers very few useful insights. It was also determined that the FDE tracks best at a smaller added moment of inertia δI and a smaller starting roll/pitch angle. In conclusion, the usefulness of FDEs was demonstrated for their ability to capture the added moment of inertia at lower damping values. Some useful new trends were also observed for coefficients a and b in the case of the particular box barge studied here.

8.2 Future Work

FDEs were applied to a very fundamental system in this thesis with the desire to determine the existence of a relationship between coefficients a and b and different variables in the equation of motion for roll and pitch. It would be worthwhile for future works to focus on a more comprehensive system and more varieties of hull forms to see if the conclusions drawn here can be generalized and whether the pattern seen in Table 5.2 is repeatable. Even on

this simpler scale, the effects of changing the metacentric height GM and the mass moment of inertia I were not fully determined. The effect of varying the roll or pitch velocity and the subsequent effect on a and b also requires research. As mentioned before, a comparison between the pitch and roll model with the number of oscillations held constant also requires work and may yield some interesting insights. Finally, a comparison to experimental data would be useful to see how much of the memory effect is in fact being captured by the FDEs.

Bibliography

[1] Assaleh, K., & Ahmad, W. W. (2007). Modeling of Speech Signamls Using Fractional Calculus, *Proc. 9th International Symposium on Signal Processing and its Applications*, 1-4.

[2] Bassler, C. C. & Reed, A. M. (2009). An Analysis of the Bilge Keel Roll Damping Component Model, *Proc. 10th International Conference on Stability of Ships and Ocean Vehicles*, Naval Surface Warfare Center, Carderock Division, USA.

[3] Dalir, M., & Bashour, M. (2010). Applications of Fractional Calculus, *Applied Mathematical Sciences*, 4(21), 1021-1032.

[4] Dalzell, J. F. (2010). A Note on the Form of Ship Roll Damping, *Journal of Ship Research*, 22(3), 178-185.

[5] Debnath, L., & Bhatta, D. (2006). *Integral Transforms and Their Applications* (2nd ed., pp. 279-282). Chapman and Hall.

[6] Froude, W. (1861). On the Rolling of Ships, *The Papers of William Froude M.A., LL.D., F.R.S. 1810-1879*. London, Institution of Naval Architects.

[7] Fujino, M., Ida, T., Maeto, T., & Numata, T., (1979). A Consideration on the Hydrodynamic Normal Forces Acting on the Bilge Keel, *JSNA Japan*, Vol. 144.

[8] Gillmer, T., & Johnson, B. (1982). *Introduction to Naval Architecture*. Annapolis, MD.: Naval Institute Press.

[9] Goda, K., & Miyamoto, T. (1975). Measurement of Pressures on Hull and Deck of Two-Dimensional Model in Large Amplitude of Oscillation, *T-West Japan SNA*, Vol. 49.

[10] Heaviside, O. (1899). *Electromagnetic Theory*, Vol. 2. The Electrician Printing and Publishing Co, London.

[11] Himeno, Y. (1981). Prediction of Ship Roll Damping - State of the Art, U. Michigan Dept. of Naval Arch. and Marine Engineering, Report 239.

[12] Ikeda, Y., Himeno, Y., & Tanaka, N. (1978). Components of Roll Damping of Ship at Forward Speed, *JSNA Japan*, Vol. 143.

[13] Kato, H. (1965). Effects of Bilge Keels on the Rolling of Ships, *JSNA Japan*, Vol. 117.

[14] Kriloff, A. (1898). A General Theory of the Oscillations of a Ship in Waves, Trans. INA, Vol. 40, 135-196.

[15] Lewandowski, E. M. (2004). *The Dynamics of Marine Craft: Maneuvering and Seakeeping*. World Scientific. Washington D. C.

[16] Ode45: Solve Nonstiff Differential Equations; Medium Order Method. (n.d.). Retrieved April 16, 2015, from http://www.mathworks.com/help/matlab/ref/ode45.html.

[17] Oustaloup, A. (1981). Linear feedback control systems of fractional order between 1 and 2, *Proc. IEEE Symposium on Circuits and Systems*, Chicago, USA, 4.

[18] Schiffmann, W. H. & Geffers, H. W. (1993). Adaptive Control of Dynamic Systems by Back Propagation Networks, *Neural Networks*, Vol. 6(4), 517-524.

[19] Sebaa, N., Fellah, Z. E. A., Lauriks, W., & Depollier, C. (2006). Application of Fractional Calculus to Ultrasonic Wave Propagation in Human Cancellous Bone, *Journal of Signal Processing*, Vol. 86, 2668-2677.

[20] Spyrou, K.J., Niotis, S., & Panagopoulou, C. (2008). Novel Modeling of Ship Rolling Based on Fractional Calculus, Proceedings, 6th Osaka Colloquium on Seakeeping and Stability of Ships, Osaka, Sec. B-5-1, 1-8.

[21] Suárez, J. I., Vinagre, B. M., Caderón, A. J., Monje, C. A., & Chen, Y. Q. (2003). Using Fractional Calculus for Lateral and Longitudinal Control of Autonomous Vehicles, *Autonomous and Control System*, Vol. 2809, 337-348.

[22] Takaki, M., & Tasai, F. (1973). On the Hydrodynamic Derivative Coefficients of the Equations for Lateral Motions of Ships, *T West-Japan SNA*, Vol. 46.

[23] Wijk, J. M. V. (2014). Added Mass Moment of Inertia of Centrifugal Dredge Pump Impellers, *Proc. ICE - Maritime Engineering*, Vol. 167(3), 135-143.

[24] Wu, J. (2001). An Experimental Method for Determining the Frequency-Dependent Added Mass and Added Mass Moment of Inertia for a Floating Body in Heave and Pitch Motions, *Ocean Engineering*, Vol. 28(4), 417-438.

[25] Xing, Z., & McCue, L. (2009). Parameter Identification for Two Nonlinear Models of Ship Rolling Using Neural Networks, *Proc. 10th International Conference on Stability of Ships and Ocean Vehicles*, Virginia Tech, Blacksburg.

[26] Yumuro, A. (1970). Research on Anti-Rolling Fin, Part 2, I.H.I. Tech. Rep., Vol. 10(2).

[27] Zubaly, R. (1996). *Applied Naval Architecture*. Centreville, MD.: Cornell Maritime Press.

Appendix A

Additional Figures

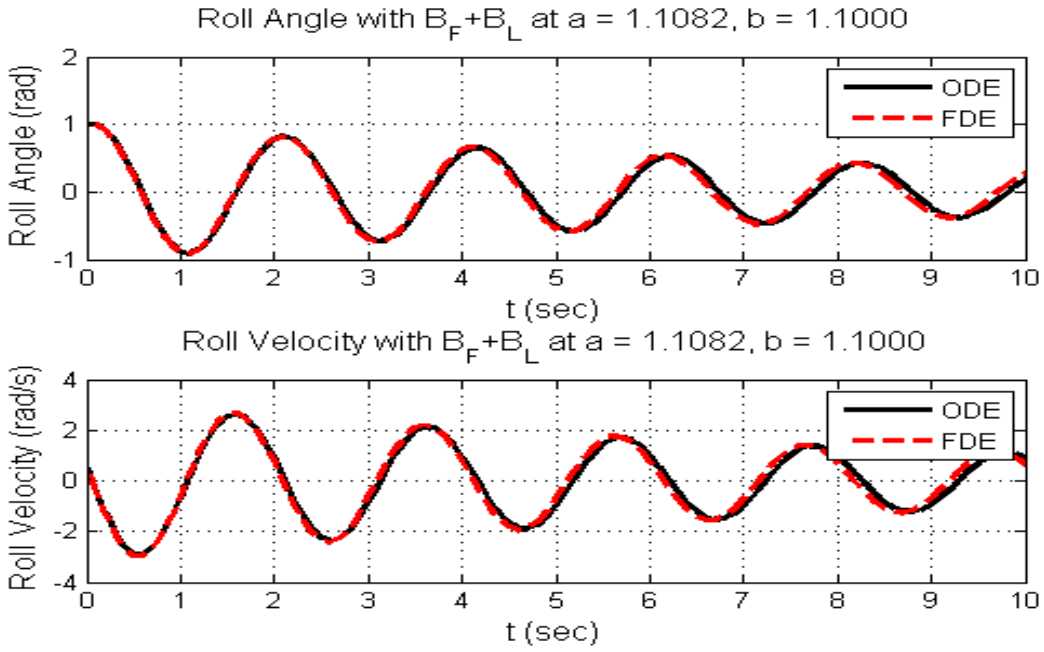

Figure A.1: Roll angle and roll velocity vs. time when damping $= B_F + B_L$

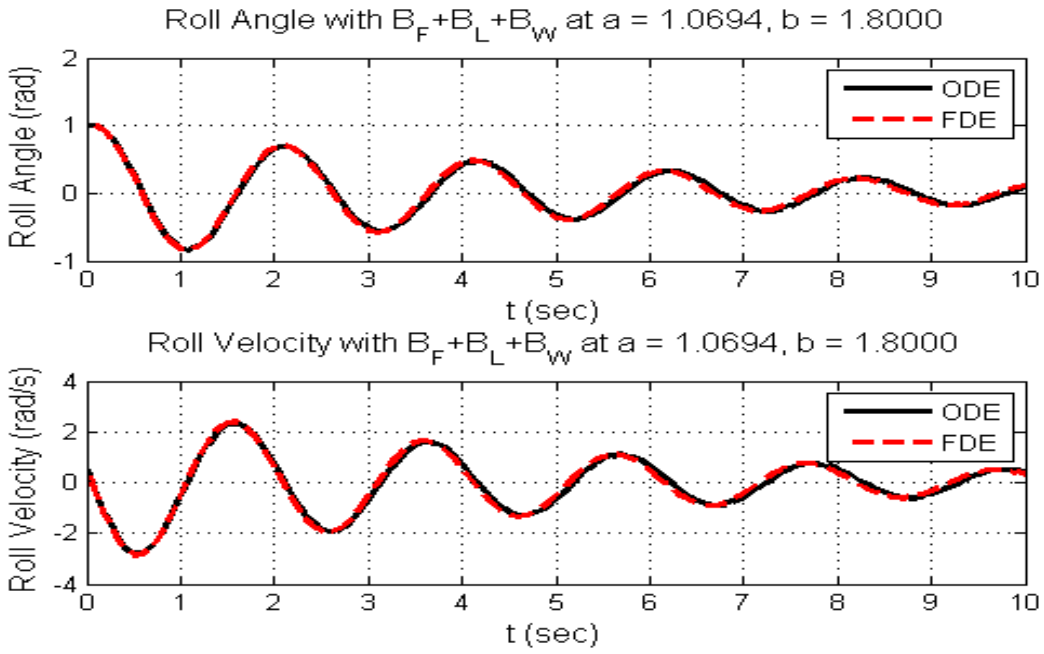

Figure A.2: Roll angle and roll velocity vs. time when damping $= B_F + B_L + B_W$

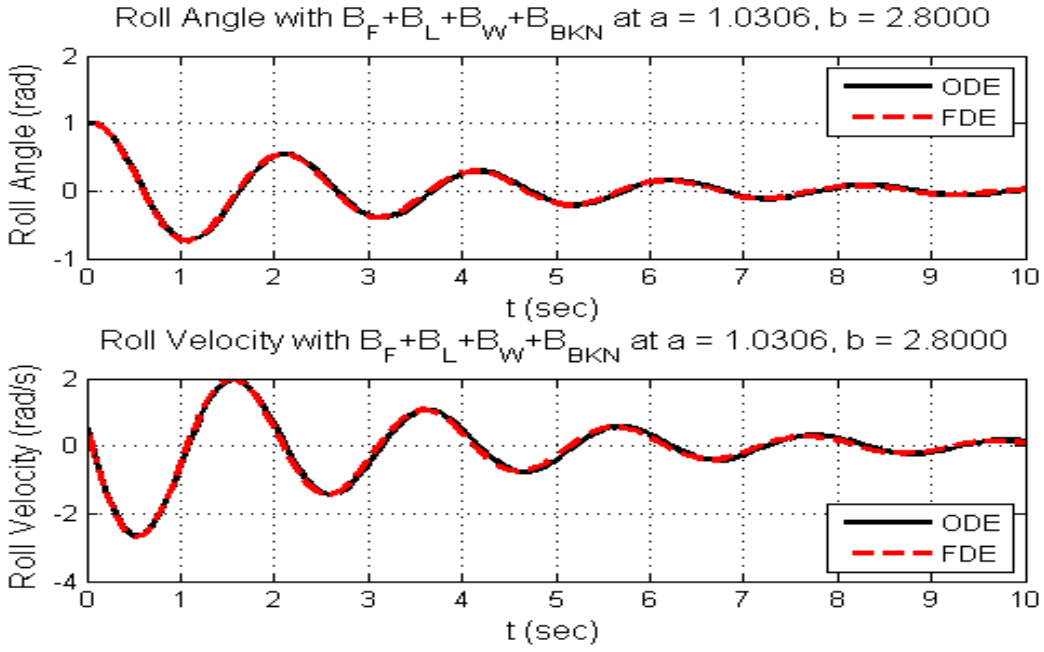

Figure A.3: Roll angle and roll velocity vs. time when damping $= B_F + B_L + B_W + B_{BKN}$